VKI TN 41

AD 674003

von KARMAN INSTITUTE

FOR FLUID DYNAMICS

GRANT AF EOAR 66-43
Scientific Report No 1

EFFECT OF SURFACE ROUGHNESS ON AXISYMMETRIC LAMINAR SEPARATED FLOWS AT M = 5.4

by

W.C. SCHNELL and J.J. GINOUX

VKI TN 41

REPRODUCED FROM
BEST AVAILABLE COPY

AUG 30 1968

This document has been approved for public release and sale; its distribution is unlimited

RHODE-SAINT-GENESE, BELGIUM

JANUARY 1968

Reproduced by the
CLEARINGHOUSE
for Federal Scientific & Technical
Information Springfield Va. 22151

GRANT AF EOAR 66-43 January 1968

SCIENTIFIC REPORT No 1

EFFECT OF SURFACE ROUGHNESS ON AXISYMMETRIC LAMINAR SEPARATED FLOWS AT M = 5.4

W.C. SCHNELL and J.J. GINOUX

von KARMAN INSTITUTE FOR FLUID DYNAMICS
Rhode-Saint-Genèse, Belgium

VKI TN 41

This document has been approved for public release and sale; its distribution is unlimited

This research has been sponsored in part by the Air Force Office of Scientific Research, through the European Office of Aerospace Research, OAR, United States Air Force, under Grants AF EOAR 66-43

FOREWORD

The work described herein was done by Mr. W.C. Schnell under the supervision of Professor J. Ginoux, in partial fulfillment of the requirements for receiving the diploma of the von Karman Institute for Fluid Dynamics. Mr. Schnell, an American student, obtained a grade of Distinction for the academic year 1966-67.

This research has been sponsored in part by the Air Force Office of Scientific Research, through the European Office of Aerospace Research, OAR, United States Air Force, under Grant AF EOAR 66-43.

ABSTRACT

The effect of controlled roughness was studied on a flared ogive cylinder at M = 5.3, with emphasis on three-dimensional perturbations at reattachment, by employing pitot pressure surveys and sublimation techniques. Cylindrical roughness elements of slightly less than the boundary layer thickness were used. Protuberance of this size were found not to contaminate the laminar reattachment compared to a model free of roughness.

The results indicated that weak disturbances upstream of separation became amplified in the free shear layer and produced significant spanwise pitot pressure fluctuation at reattachment. Results of a systematic investigation of the effects of roughness height, diameter and spacing are presented.

TABLE OF CONTENTS

LIST OF TABLES

LIST OF FIGURES

LIST OF SYMBOLS

C	Chapman-Rubesin constant
d	Diameter of roughness element
K	Height of roughness element
L	Distance to flare-cylinder junction as in figure 1.
ΔL	"Nick" in leading edge
ℓ_0	Distance of non-interaction between two perturbations
ℓ_s	Separation length as defined on page 15
P	Static pressure
P_0	Stagnation pressure
P_p	Pitot pressure
ΔP_p	Difference between peak and valley pressure levels
$r(x)$	Axisymmetric corss section radius
Re	Reynolds number
T	Static temperature
t	Time
T_0	Stagnation temperature
T_r	Recovery temperature
T_w	Wall temperature
U	Velocity at edge of boundary layer
u	Boundary layer velocity component parallel to surface
$\vec{u}$	Velocity (vector) induced by vortex motion
w	Distance from valley to adjacent mean
X	Streamwise coordinate along body surface
X_f	Flare station measured from junction
y	Coordinate normal to body surface
α	Cone angle
γ	Ratio of specific heats
δ	Boundary layer thickness
ε	Leading edge thickness

$\Delta\varepsilon$	"Groove" in leading edge
λ	Wavelength of perturbation as defined on page 24
θ	Flare angle
θ_{RE}	Angle between roughness elements
ϕ_{RE}	Distance between peaks corresponding to roughness elements (ideally $\phi_{RE} = \theta_{RE}$)
ν	Kinematic viscosity

Note 1 : Angular-displacement conversion

A θ_{RE} displacement corresponds to $0.262\ \theta_{RE}^{\circ}$ mm

A ϕ_{RE} displacement corresponds to $0.330\ \phi_{RE}^{\circ}$ mm at flare station $X_f = 30$

Note 2 : Unless otherwise specified all dimensions are in millimeters.

I. INTRODUCTION

One of the most important factors affecting the spanwise distribution of boundary layer properties (i.e. heating rate) is the condition of theleading edge or the body surface. Irregularities such as expansion slots (envisioned as necessary in winged re-entry), connecting rivets, or distortions due to the high temperature buckling may well be prominent factors in determining the nature of the spanwise boundary layer distribution. Since it is possible that surface irregularities may appreciably affect the heat transfer distribution across a span, the designer of winged re-entry configurations must be able to estimate the extent to which these irregularities influence the downstream boundary layer distribution. The purpose of this report is to present the results of an experimental study of two types of surface distortion, finite leading edge and controlled surface roughness on a reattaching boundary layer.

In the course of a previous research program undertaken at von Karman Institute on laminar separated supersonic flow, Ginoux found that three-dimensional perturbations existed in the reattachment region of the flow over backward facing steps (refs. 1, 2,3). It was concluded that this phenomenon was essentially one of instability in the two-dimensional flow, the main triggering action arising from small irregularities in the leading edge. It was further shown that these perturbations were fundamental to separation in general as they were observed in various types of separated flow (rearward and forward facing steps, ramps, cavities, shock wave boundary layer interaction) over a range of Mach numbers (1.5 to 7.0). Later research, by Ginoux, employing total-head and static probe surveys at various heights in the reattaching boundary

layer of stepmodels resulted in determining the nature of these three-dimensional perturbations (ref. 4). In fact the disturbances at reattachment proved to consist of a row of counter-rotating streamwise vortices generally located within the boundary layer. In this same research, to ease the experimental study, the amplitude of the flow perturbations was varied artificially by gluing thin strips of cellulose tape to the model surface in the vicinity of the leading edge. A transient calorimetric technique was used in determining the effect this small artificial roughness had on the heat transfer rate at reattachment. These local heat transfer measurements showed that the vortices produced very large peaks locally in the heating rate, much larger than the usually measured turbulent value after transition.

Previous investigation has thus demonstrated the existence and important significance (i.e. : peaked heating) of three-dimensional perturbations in a reattaching boundary layer on two-dimensional models. It has also been shown that the leading edge acts as a mechanism which initiates these perturbations. It is clear therefore that a two-dimensional configuration is not ideally suited for a detailed study of controlled roughness for it is not intrinsically vortex-free. Thus the impetus is given for the study of an axisymmetric configuration whereby the finite leading edge is replaced by a point.

This report is intended to verify, by comparison of hollow and closed nosed axisymmetric models, that a pointed axisymmetric configuration is ideally suited for studies of controlled roughness since it gives rise to a vortex-free environment.

Ultimately the effect of introducing various sizes of three-dimensional roughness (cylinder) at different spacings will be examined in the reattachment region.

2. APPARATUS

2.1. Wind Tunnel

The test program was conducted in the VKI H-1 hypersonic wind-tunnel in a contoured rectangular nozzle at M = 5.4. The size of the test section was 14 x 14 cm^2 and the flow was uniform within 1 % in Mach number. Running times up to 3 minutes were available at tunnel stagnation pressure of 12 to 32 kilogram-force per square centimeter absolute and with stagnation temperature of 160°C to 250°C.

The H-1 facility is equipped with a double-pass schlieren (either continuous or instantaneous light source) system and an instantaneous-spark shadowgraph system. Both optical systems make use of conventional spherical mirrors.

An incidence mechanism is an integrated feature of the tunnel so that angle of attack may be adjusted.

2.2. Models

Two basic model designs were employed : flared hollow cylinder and flared ogive cylinder configurations. The geometry, dimensions and designations of the various models are given in fig. 1. All models were constructed from stainless steel.

Preliminary tests were conducted on both basic model designs in order to exmaine the flow field dependence on flare angle and position. For this study movable flares were emloyed so that a range of 40 millimeters could be covered.

For the roughness tests only the nosed configuration was employed. Its design was such that the nose could be removed tc make possible the introduction of narrow rings on which roughness elements had been installed. The dimensions of the roughness elements and the ring designations are given in fig. 2. The roughness elements consisted of certain diameter wire force fitted into holes drilled in the ring and then cut or filed to the desired height. Fig. 3 shows model 0C-II with nose slightly unscrewed to illustrate the installation of roughness ring RE-8.

2.3. Instruments and Instrumentation

A small 24 volt DC electric motor was used to rotate the model at a constant angular velocity of 0.6° per second over a range of 110° in either direction. The motor-model integration is shown in fig. 3.

A single pitot probe was attached to the overhead tunnel wall in such a manner that it could be manually moved, by means of a worm-gear mechanism, normal to the flow. The probe had outside and inside diameters of 0.8 and 0.6 millimeters respectively. Two electrical pressure transducers with ranges of 100 and 1000 millimeters of mercury were referenced to vacuum, atmosphere, or a certain tank pressure depending upon the sensitivity and total head level desired. The electrical outputs of the transducers were recorded on a digital readout recorder and/or a graphispot chart recorder.

Four alignment pressure taps, at 90° intervals, were positioned 20 millimeters from the flare end. These static pressures were measured by connecting the orifices to a

pressure switching device which in turn connected the orifices to the 0-100 mm Hg transducer described above, whose electrical output was fed to the digital readout recorder.

3. MEASUREMENTS AND TEST TECHNIQUES

3.1. Flow Visualization

For the laminar-transitional study presented in section5, it was necessary to visualize the flow field of different model configurations over a range of Reynolds numbers. An indication of different flow regions was obtained from the schlieren and shadow pictures. These two optical techniques were especially necessary in the determination of the separation length, by measuring the distance between the separation and reattachment shocks, as they appeared on the photographs.

Visual indications were obtained of the spanwise variations of boundary layer properties by the sublimation technique in which a volatile chemical solid is sprayed over the model surface, and upon exposition to the airstream sublimes at a rate proportional to the local skin friction coefficient (assuming a constant wall temperature). The diffusible solid and the solvent used in this investigation were acenaphtene and petroleum ether respectively. This saturated solution has been sucessfully used for running times of up to two minutes. In order to improve the method, the surface of the models was first sprayed with tracing blue ink and then the acenaphthene in order to yield a good contrast between regions of high and low sublimation rates.

3.2. Total Head Surveys

Total head surveys were obtained in a transverse plane as the model was rotated by the electric motor described in section 2. Although the probe was fixed, surveys were made at

different stations (both after and before separation) by moving the model either forward or rearward in the uniform flow produced in the test section. Different heights in the boundary layer were surveyed by employing the manually operated worm-gear mechanism. Measurements were obtained on both the ogive cylinder with and without roughness rings and the hollow cylinder.

4. PRECISION AND ACCURACY

4.1. Optical Techniques

The study of section 5 required extensive use of the schlieren and shadowgraph techniques. It is noted that the location of transition and separation length varied between the two techniques; however, interest was centered on trends rather than absolute magnitudes, and in this aspect both optical methods were complementary.

4.2. Sublimation Technique

A dissolved chemical solid sublimes at a rate proportional to the local skin friction coefficient if the wall temperature is constant. Such an isothermal condition cannot be achieved in the H-1 facility at practical running times. However it is noted that the present investigation does not deal with streamwise but instead with transverse variations, which are validly observed irregardless of a non-uniform sublimation rate.

4.3. Pressure Measurements

Unless otherwise specified all tests were conducted at a stagnation pressure of 15.2 ± 0.2 kg/cm^2. The small variation was not accounted for since rigorous quantitative measurements were not sought in this investigation.

The error in static and pitot measurements is considered to be 1 percent at most. The accuracy of the pressure transducers is approximately 1/2 percent of full scale reading, and a calibration error of 1/2 percent is considered an upper limit.

Interest was placed on a quick probe response rather than small probe diameter. Upon examining the response time it was observed that the probe produced an accurate reading within 1 percent of the asymptotic value in less than 1/2 second. This corresponds to only 0.2 degrees of angular rotation of the model which is considered negligible.

4.4. Temperature Effects

Owing to the relatively large stagnation temperature compared to ambient temperature the recovery temperature was never reached during test running times. Thus a gradient in wall temperature with time always existed producing heat transfer from the boundary layer to the model surface. Significant boundary layer growth (estimated to be 20 percent on the flare in appendix IV) occurred during each run. The result is that the probe location relative to the boundary layer gradually decreases during the course of a test producing a falling mean pressure. See fig. 4. Correspondingly the boundary layer profiles (pressure) initially and at the end of each test reflect this difference as shown in fig. 5. This gradual drop in pressure level is not considered important for the range of boundary heights investigated especially since interest was centered on fluctuations of the mean rather than the absolute value of pressure level.

However the effect of boundary layer growth upon the roughness height compared to boundary layer thickness could be significant since the ratio of k/δ would decrease during a test. The effectiveness of a protuberance in disturbing the flow is therefore greatest initially and then gradually falls off. This phenomenon was observed qualitatively but not quantitatively.

Future investigators should consider this effect of temperature.

4.5. Allignment

Allignment pressure taps were initially employed to center the model so that cross flow could not contaminate the separated region. This precaution was subsequently eliminated after sublimation tests verified that a misallignment of at least 0.8 degrees or less did not introduce observable perturbation.

4.6. Model Construction

Difficulties were encountered in the construction of roughness rings due to the small size of the protuberances. Under magnification (x100) it was found that the roughness elements varied by 10 percent in height and 5 percent in diameter (for the most common size (K = .2, d = .5) in some instances. An error in effective area of 15 percent for a particular element would not be uncommon. This was considered unimportant for the tests investigating spacing since only a physical appreciation for the phenomenon was sought. However for the investigation of protuberance size (ring RE-VD8) care was taken, employing the microscope, to record the exact dimensions of each roughness element.

5. GENERATION OF LAMINAR FLOW FIELD

The objective of this investigation was to examine the effect of discrete roughness elements in a laminar reattachment region. It was therefore necessary to obtain a reattaching boundary layer that was fundamentally laminar. This laminar condition was to be satisfied not only on models free of roughness elements but also with the roughness rings introduced.

Because of the difficulty in determining, from flow visualization photographs, the fine gradation between laminar and transitional flows, it became desirable to employ the following criterion (ref. 5) in determining the types of reattachment that existed on the HC and OCI models. This criterion specifies the manner in which the separation length, ℓ_s, varies with Reynolds number. In this paper the separation length is defined as the distance, along the body surface, between the separation and reattachment shocks when they are extrapolated to the model wall. It was observed for the HC and OCI models that the extrapolation point of the reattachment shock generally coincided with the flare cylinder junction within the error of measurement. To ease the investigation, the separation length was taken to be the distance between the extrapolated separation shock and the junction.

The dependence of separation length on Reynolds number is such that for laminar reattachment the relationship is direct while for transitional reattachment it is inverse.
See below.

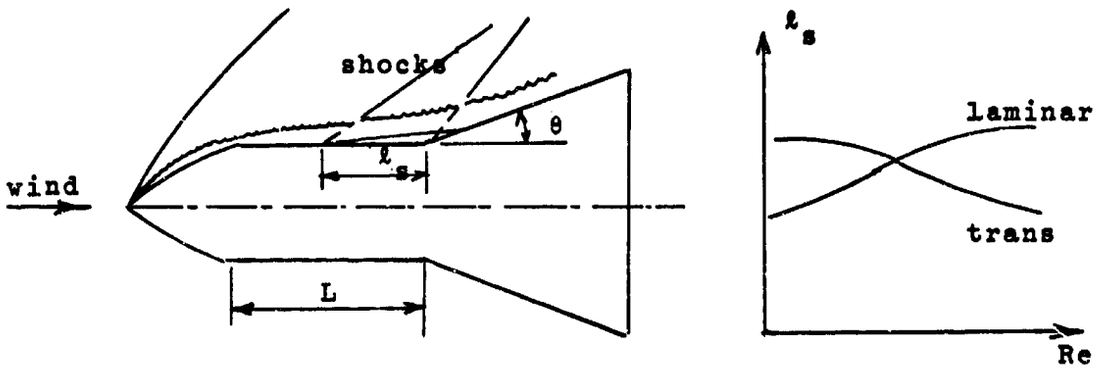

5.1. Without Roughness

Preliminary tests were conducted on HC and OCI models in order to determine an optimum model geometry on which laminar reattachment could be assured. An upperbound on cylinder length, L, and flare angle, θ, was sought so that the boundary layer would exhibit sufficient growth and so the ensuing separated region would have reasonable size.

Each model configuration (18 in total) was run at four different Reynolds number levels, the Reynolds number being varied through its dependence on stagnation pressure. For each configuration both schlieren and shadowgraph pictures were obtained at each Reynolds number. The separation length was carefully measured on each photograph and plotted against Reynolds number. The curve for each model configuration was obtained by observing the trend of both schlieren and shadowgraph data which complemented each other. The results for the 7 1/2° flare models are presented in fig. 6. A table summarizing the type of flow reattachment is shown below. (All 5° flare models exhibited laminar reattachment).

Model	θ	L	Laminar	Lam-(Low Re) Trans-(High Re)	Transitional
HC-2	7 ½	20	x		
-5		40		x	
-8		60			x
OCI-2	7 ½	20	x		
-5		40	x		
-8		60		x	
HC-3	10	20	x		
-6		40			x
-9		60			x
OC-3	10	20	x		
-6		40		x	
-9		60		x	

On the basis of these results, models HC-5 and OCI-5 (becomes OCII) were selected for the continuation of the research, for they both exhibit laminar reattachment at low Reynolds numbers especially. The flow field over these optimum models is seen on schlieren and shadowgraph pictures in fig. 7.

5.2. With Roughness

The same criterion was employed to determine if a typical roughness element could significantly infuence the upstream transition movement such that it would contaminate the laminar reattachment. A single protuberance of diameter 0.5 millimeters and height 0.2 millimeters was chosen . This

height was found to be slightly less than the calculated boundary layer thickness of 0.22 millimeters at the roughness location (see appendix I).

Shadowgraphs were obtained for the flow over model OCI-5 with the roughness element in a vertical longitudinal plane. The results which indicate a laminar reattachment are tabulated below.

P_0	ℓ_s
24.2	20.6
22.6	19.6
17.4	17.1
12.8	EST. $16\frac{1}{2}$ *

* At low stagnation pressure levels it becomes difficult to observe the shock pattern.

In support of this result, Holloway and Sterret (Ref.6) have reported that transition may be delayed slightly when the surface roughness is less than the boundary layer thickness.

Although the single roughness element appeared not to influence the forward movement of transition, it was anticipated that the spacing of several elements might affect the transition location. This was not verified in the H-1 facility; however, the data of reference 7 indicates that the lateral spacing of a single row of roughness elements (spheres) has little effect on boundary layer transition provided the spheres are not so close together that a two-dimensional roughness is approximated. Reference 8 shows, for subsonic flow,

that a spanwise spacing of projections equal to 3 times the projection diameter had no effect on the critical roughness height as compared with a single projection. This may not be strictly true for supersonic speeds where the kinematic viscosity varies with temperature in addition to the velocity variation. Nevertheless Braslow reported (ref. 8) that the transition triggering mechanism of three-dimensional protuberances appeared to be the same at supersonic and subsonic speeds.

On the basis of the above it was expected that roughness elements of height 0.2 millimeters or less did not contaminate the laminar reattachment of model OCII.

6. PHYSICAL INTERPRETATION OF SPACING EFFECT

It has been shown that the three-dimensional perturbations existing at reattachment are actually pairs of counter-rotating vortices (ref. 4). Consider how such a pair of vortices affects the boundary layer by analyzing the induced velocity at points A, B and C shown below*.

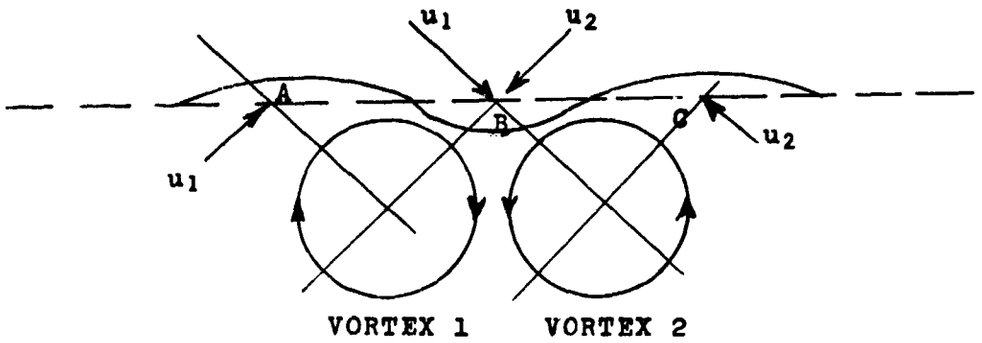

The induced velocities are as shown. The boundary layer at A and C tends to thicken while at the center point B it becomes thinner. The deformation theoretically is greater between the vortices at B since there the induced velocities complement each other.

Consider a small two-dimensional protuberance on a body surface subjected to an airstream. The air must separate in order to flow over the obstacle thus generating a region or reversed flow as shown below.

* It is also noted that a single vortex could affect the boundary layer profile as well.

For the three-dimensional roughness case this separated region, in which a vortex-type pattern is produced, must "wrap itself around" the projection and consequently travel downstream as shown below.

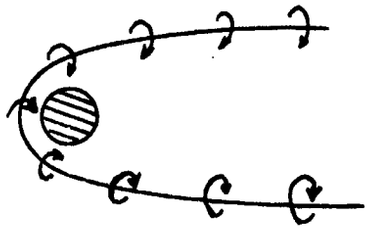

The downstream pattern appears to result in a pair of counter-rotating vortices. If this is true the boundary layer will exhibit "waviness" (described earlier) due to the presence of the protuberance.

Consider a typical profile for points A (or C) and B with respect to an undisturbed one. The boundary layer thickness at A will be greater while at B it will be less, due to the influence of the vortices. Ginoux has shown (ref. 3) that the slopes of the deformed profiles must be as indicated below. This has also been verified in the present investigation by utilizing results from sublimation tests.

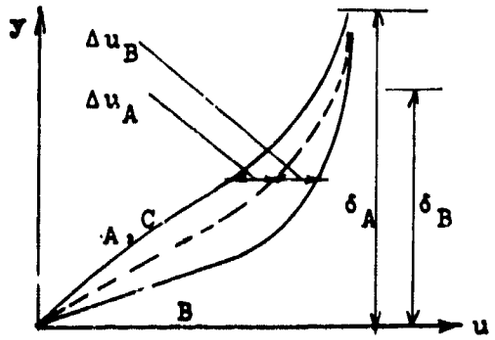

$$\delta_A > \delta_B$$

$$U_A < U_B$$

$$P_{pA} < P_{pB}$$

$$\frac{\delta u}{\delta y}_A < \frac{\delta u}{\delta y}_B$$

From the above it follows that the percent amplitude fluctuation ($\Delta u/u$) between points A and B will be greatest in the mid-region

of the boundary layer. It is therefore expected that spanwise pitot surveys across a pair of vortices would be a successful means of detecting the influence of a roughness element, in which case a "valley-peak-valley" distribution would result for points A, B, C respectively. Although the velocity fluctuation dies out near the wall ($\frac{\Delta u}{u} \to 0$), the slopes of the two profiles differ markedly as $y \to 0$ so that the sublimation technique may be employed in analyzing a roughness element's influence on transverse boundary layer properties.

Consider two equal sized roughness elements spaced far apart so that one has negligible influence upon the other. The idealized model of the pitot pressure variation is shown below; note that this is roughly the inverse of the deformed boundary layer thickness.

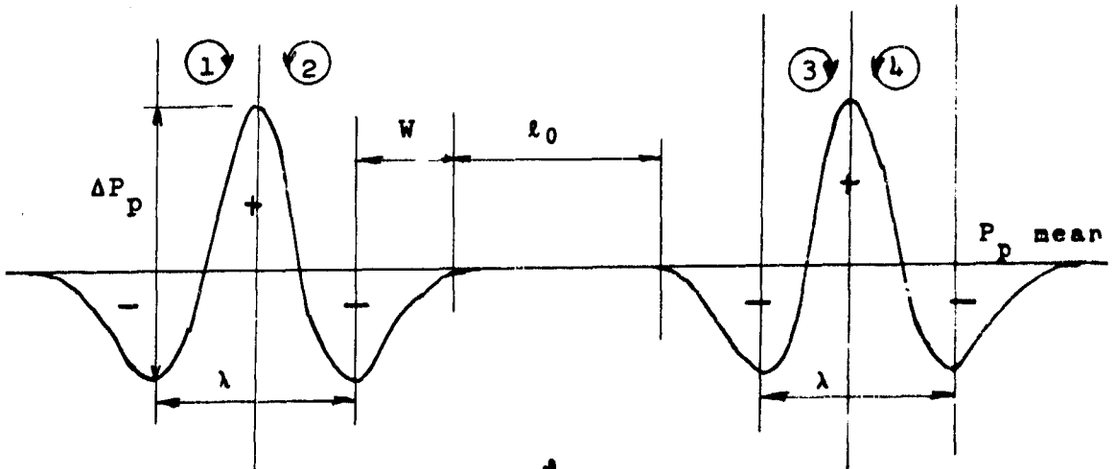

It is interesting to consider the possibility of moving the roughness elements closer together. For $\ell_0 > 0$ vortices 2 and 3 do not interact with each other assuming

that no secondary vortices are induced by the original pair of vortices considered above. The condition $\Delta_0 = 0 (\phi_{RE} = \lambda + 2w)$ is termed "just critical". For less than the critical spacing the profile is expected to assume various shapes depending upon the mutual influence of vortices 2 and 3. The most interesting interaction case is expected to occur when the two adjacent valleys are superimposed ($\theta_{RE} = \lambda$ or $\Delta_0+2w=0$). This situation in which the two valleys appear to be complementing each other (note that vortices 2 and 3, because of their proximity, might now be considered a counter-rotating pair) is termed "total reinforcing". These and other intermediate possible angular spacings are considered in fig. 8.

7. DATA REDUCTION

For the hollow cylinder it was of interest to measure the maximum percent fluctuation on the mean and the wavelength. The maximum percent fluctuation is denoted by $(\Delta P_p/P_p)_{max}$ where the mean is defined as the average of the peak and neighboring valley pressure levels of the fluctuation yielding the greatest pitot pressure difference. The wavelength, λ, is defined as the ratio of a certain basic spanwise length (or arc) divided by the number of peaks, or valleys, recorded along that length. The ratio of wavelength to the calculated boundary layer thickness (see appendix II) was obtained in order to compare with the results of reference 2.

For the roughness model, OCII, interest was centered on the percent amplitude fluctuation and the "valley wavelength" of a roughness element profile. The percent fluctuation is $\Delta P_p/P_p$, and the "valley wavelength", λ, of a given protuberance is the distance (or arc) between the two valleys that flank the parent peak.

8. RESULTS AND DISCUSSION

8.1. Hollow Cylinder

The complete data and test conditions are shown in table 1. Typical pitot pressure variations with relative angular position are illustrated in figure 9 and results from sublimation tests are shown in figure 10.

It is especially noted that significantly large perturbations exist at reattachment; a maximum fluctuation of 50% or more is not uncommon. It was reported in ref. 5 that in some cases pitot pressure spanwise variations were as large as 50% of a reference value on the centerline of two-dimensional step models.

It is to be observed that maximum and minimum pressure differences appear to be very irregular; however, the displacements between the pressure peaks (wavelength) seem to be roughly equal (note test F260 in particular). The number of these peaks is in agreement with the number of striations detected on the model surface with the sublimation technique. This can be seen by comparing Tests F56, 110, 225 (Table 1) in which the same leading edge condition existed.

The ratio of wavelength to boundary layer thickness (calculated in Appendix II) is to be compared with Ginoux's backward facing step data. In the reattachment region at x_f=30 the non-dimensioned wavelength is shown versus leading edge condition in the chart below.

L.E.	λ	λ/δ
.06 (OLD)	2.5	3.2
.06 (NEW)	2.2	2.9
↓	2.2	2.9
↓	2.1	2.8
.02	1.9	2.5

Ref. 2 reports, for "moderate" separated flows, that the ratio of wavelength to boundary layer thickness at separation has a range of about 2 to 3 1/4. The results of this research are in good agreement.

It would be interesting to investigate the dependence of wavelength upon leading edge condition and flare station. From Table I speculation on these two relationships is possible (see Project Report 67-171); however, it certainly would not be conclusive. Suffice it to say that further data must be obtained in these areas.

The most unquestionable result obtained from hollow cylinder tests is also the most important. Strong perturbations exist at reattachment which are triggered by inaccuracies in the machining of the leading edge (as explained in ref. 3). These strong total head variations indicate that the boundary layer profiles are distorted in such a manner that the boundary layer exhibits waviness.

This study has verified that axisymmetric configurations featuring leading edges are poor specimens on which to study the effects of controlled roughness for the flow is not free of three-dimensional perturbations.

8.2. Ogive Cylinder

8.2.1. Without roughness

A spanwise pitot survey and the sublimation technique have demonstrated that a closed nosed configuration is entirely free of three dimensional perturbations. These results are shown in figs. 11 and 12 respectively. Comparison with the results of figs. 9 and 10 for the hollow cylinder illustrates the contrast. The results of the pitot survey indicates that a maximum fluctuation of only 2% exists at reattachment on the ogive cylinder compared to 50% on the hollow cylinder.

It is therefore clear that a closed nosed configuration is ideally suited for roughness studies since it is intrinsically free of three dimensional perturbation. This is an agreement with the earlier observation made by Ginoux in ref. 5.

8.2.2. Preliminary investigations - Rings RE-8,16,32

Prior to the formal investigation of controlled roughness, rings RE-8, 16, 32 were subjected to total head surveys and sublimation tests. Typical pressure distributions are shown in figs. 13, 14, 15, respectively, while the complete data is reduced in table 2. Photographs of the sublimation results appear in fig. 16.

For roughness ring RE-8 ($\theta_{RE}=45°$) equal sized protuberances are so spaced that the vortices of one do not interact with those of another (see fig. 13). The typical valley-peak-valley distribution anticipated in section 6 has resulted for a single element. Notice that the sublimation technique produced a light-dark-light contract which must

necessarily match the valley-peak-valley distribution of pitot pressure.

To reiterate, the peak and striation (dark line of a sublimation test) result from a depression in the boundary layer due to the action of a pair of counter-rotating vortices. The boundary layer velocity profile is deformed such that its magnitude, at any given height, is increased (producing the peak) and its slope at the wall is greater (producing the striation) compared to an undisturbed profile.

From fig. 13 the "just critical" condition, below which disturbances from neighboring elements interact, can be calculated as explained in section 6. The result for the element size employed on RE-8, 16, 32 (K=0.2, d=0.5) is θ_{RE}=21 1/2 degrees. Thus RE-16(θ_{RE}=22 1/2°) should almost demonstrate the just critical condition while RE-32 (θ_{RE}=11 1/4°) should certainly exhibit interaction. Inspection of figs. 14 and 15 supports this contention which will be considered in greater detail when the results of variable spacing are discussed.

It is interesting to note how well the sublimation results match the total head distribution. For ring RE-16 the "light-medium-light-very dark-light" striation scheme corresponds exactly to the "valley-small peak-valley-large peak-valley" pressure variation. The equally spaced striations of ring RE-32 fit well with the alternating peak and valley pressure distribution.

8.2.3. Measurements upstream of separation

Figure 17 shows the results of spanwise pressure distribution, ahead of separation for ring RE-32. The reduced data appears in Table 2.

It is first noticed that the amplitude of the fluctuations is greatly reduced compared to those observed at reattachment ($\Delta P_p/P_p$ is of the order of 10 percent before separation while at reattachment it is about 50 percent). Secondly it is observed that the wavelength is unaffected by separation being about 11 degrees in both cases. Also the wavelength appears to be almost invariant with the mean or position in the boundary layer even though the amplitude is sensitive to location. It may be that a perturbation is "born" with a certain wavelength which it retains independent of amplitude attenuations.

It is concluded that a small roughness element initiates a weak perturbation of a given wavelength. The mechanism of separation then amplifies this disturbance to produce a strong fluctuation of the same wavelenth at reattachment. It is, however, unclear how the free shear layer amplifies a disturbance and more research is required to explain this.

8.2.4. Effect of roughness size

The influence of roughness size on the vortices at reattachment was conducted using the variable dimension roughness ring, RE-VD8. The pitot pressure distributions are presented in figs. 18, 19, 20, and the data is reduced in Table 3. For this analysis the independent variables are the height, k, and diameter, d, of a protuberance, while the dependent variables are the percent fluctuation, $\Delta P_p/P_p$, and wavelength, λ

Because of the odd dimensions, due to machining difficulties, it is possible to investigate the effect of variable height for elements of similar diameters in only

three instances. This is presented in tabular form in Table 4. It is observed as K decreases both $\Delta P_p/P_p$ and λ decrease as well*. It is therefore concluded that both percent fluctuation and wavelength vary directly as roughness height for a fixed diameter.

It is possible to compare the effect of varying the roughness diameter at three different levels (approximate) of roughness height. See Table 5. In each of the three height levels it is seen that the percent fluctuation and wavelength both decrease with diameter for height roughly constant. It is concluded that the two dependent variables, $\Delta P_p/P_p$ and λ, are related directly to roughness diameter for elements of equal height.

Therefore it is seen that <u>both</u> disturbance properties, λ and $\Delta P_p/P_p$, are directly related to <u>both</u> the independent variables, k and h. Thus it is not possible to simply link amplitude to height and wavelength to diameter, as intuition might suggest.

---

* The only flaw in this trend is the value of percent fluctuation for the smallest height (the value of 33 1/2 seems too high). This is explained by observing that significant variations occasionally occurred between indentical tunnel tests. Notice that test F252 produced an unusually high value (38 1/2) for the element of height equal to .164. On rechecking test conditions it was noticed that F252 was run at a substantially lower than normal stagnation temperature. This would have the effect of increasing the Reynolds number which in turn decreases the boundary layer thickness. Thus the ratio of K/δ effectively increases and the flow views the protuberance as a greater obstacle.

8.2.5. Effect of roughness spacing

The effect of roughness spacing is considered in terms of the physical interpretation of section 6. The variable spacing roughness ring, RE-VS16, was tested at two reattachment stations (X_f = 20 and 30) in order to yield more detailed information than the previous rings (RE-8, 16, 32) provided. The pressure distributions of RE-VS16 are presented in figures 21, 22, 23, 24.

The influence of angular spacing is analyzed over a range of 45 to 6 degrees, as illustrated in the following table.

θ_{RE} tested	θ_{RE} calculated	Figure	Approximate Description
45	$\theta_{RE} > 21\ 1/2$	13	Non-interaction
22 1/2	21 1/2	14	Just critical
18	18	21	Partial interference
15	15	22	Total interference
11 1/4	12	15	Partial reinforcement
8	8	23	Total reinforcement
6	7	24	3-D to 2-D transition

The interpretation of section 6 , expected to be qualitatively valid assuming that the roughness elements are not so closely spaced that they begin to approximate a two-dimensional roughness (i.e. : a band). Braslow (ref. 8) presents results indicating that a critical spacing exists such that two-dimensional effects begin to occur. For the 0.5 millimeter diameter roughness considered in this discussion the critical spacing for model OCII

is about 7 degrees. Thus for the smallest spacing shown in the above table, explanations other than those of section 6 are necessary.

For θ_{RE}=45 degrees a considerable region of no interaction exists between the disturbances at reattachment. Based upon the pressure distribution in figure 13 it was possible to estimate θ_{RE}, using the physical model of section 6, for each of the types of interaction described in the above table.

The results for θ_{RE}=22 1/2 degrees illustrate that the valley-peak-valley distribution of one element is immediately followed by another. Note the short "return to the mean" pressure between adjacent valleys of consecutive roughness elements which agrees with the "just critical" condition of figure 8a.

For θ_{RE}= 18 degrees it is observed that the small peak is depressed some what below the mean. It seems that the influence of vortices 2 and 3 (figure 8b) is now overlapping to induce an upward shift in the boundary layer thus suppressing the small pressure peak.

As the spacing further is decreased the influence of vortices 2 and 3 is expected to increase. At an angular spacing of 15 degrees the small peak should be almost completely damped. Figure 22 indicates that total interferences is on the verge of being achieved. Only a minute peak,well below the mean, exists in the hollow of the valley.

At a spacing of the 11 1/4 degrees, the result is the oscillatory peak-valley scheme predicted in figure 8c . Vortices

2 and 3 must now be so close, that all the boundary layer between them senses the induced upwash thereby causing the distinct valley in pitot pressure.

The results for the total reinforcing condition illustrate an experimentally perfect sinusoidal pattern. Note on figure 23 for the test at $X_f = 30$ (where the mean was recorded both before and after the affected region) that the alternating peaks and valleys are not only equal in magnitude (relative to the mean) but also equally spaced. The interpretation of section 6 is again found to be satisfactory. It must now be the situation such that vortices 2 and 3 constitute a counter-rotating pair (of opposite sense) in addition to vortex pairs 1-2 and 3-4 (see fig. 8e).

As previously indicated spacings of 7 degrees or less are expected to result in disturbances that can only be explained when two-dimensional effects are taken into account. This is apparent on comparing the distribution for $\theta_{RE} = 6$ degrees with that of $\theta_{RE} = 8$ degrees. It is observed that the second of the three peaks is considerably reduced to approximately the mean value. It appears that this smaller peak becomes "compressed" owing to the proximity of the two outer peaks. Possibly such closely place roughness elements "throttle" the flow passing between them thus producing weaker vortices. Further research employing many more than three protuberances at the 6 degrees spacing is required to demonstrate this.

The distribution of pitot pressure for the case described as total reinforcement (figure 23) is the experimentally desirable one. A respectable and regular spanwise distribution of alternating peaks and valleys with equal amplitude and wavelength was sought and achieved. It is concluded that it is possible to artificially create a homogeneous peak-valley pattern around the circumference of a nosed axisymmetric configuration.

CONCLUSIONS

1. Pitot Pressure surveys and sublimation tests were successfully conducted on hollow cylinder and closed nosed axisymmetric models that exhibited laminar reattachment.

2. It was verified that an ogive nosed axisymmetric configuration is ideally suited for an investigation of controlled roughness since it gives rise to a vortex-free reattaching flow.

3. It was shown that variations in roughness height or diameter could influence both the amplitude fluctuation and the wavelength of perturbations at reattachment.

4. By controlling the roughness spacing it was demonstrated that various spanwise pitot pressure profiles could be artificially simulated. In particular a repeatable and regular spanwise distribution of alternating pressure peaks and valleys of equal magnitude was produced at reattachment.

REFERENCES

1. Jean J. GINOUX : Experimental Evidence of Three-Dimensional Perturbations in the Reattachment of a Two-Dimensional Laminar Boundary Layer at M = 2.05.
V.K.I. TN 1, November 1958.

2. Jean J. GINOUX : Laminar Separation in Supersonic Flow with Emphasis on Three-Dimensional Perturbations at Reattachment.
V.K.I. TN 3, February 1960.

3. Jean J. GINOUX : Leading Edge Effect on Separated Supersonic Flows.
V.K.I. TN 4, May 1961.

4. Jean J. GINOUX : Streamwise Vortices in Laminar Flow.
AGARDograph 97, Part I, May 1965.

5. Jean J. GINOUX : Investigation of Flow Separation over Ramps at M = 3.
AEDC - TR - 65 - 273, December 1965.

6. P.F. HOLLOWAY & J.R. STERRET : Effect of Controlled Surface Roughness on Boundary Layer Transition and Heat Transfer at Mach numbers of 4.8 and 6.0.
NASA TN D-2054.

7. E.P. DRIEST & W.D. McCAULEY : The Effect of Controlled Three-Dimensional Roughness on Boundary Layer Transition at Supersonic-Speeds.
Journal Aero/Space Sciences, Vol. 27, April 1960.

8. A.L. BRASLOW : Review of the Effect of Distributed Roughness on Boundary Layer Transition.
AGARD Report 254, April 1960.

9. J.V. BECKER & P.F. KORGCINSKI : Heat Transfer and Pressure Distribution at a Mach number of 6.8 on Bodies with Conical Flares and Extensive Flow Separation.
NASA TN D-1260, April 1962.

APPENDIX I

A very first order analysis is presented for the estimation of the boundary layer thickness at the roughness location. Instead of the ogive nose (which develops a negative pressure gradient) a conical nose is assumed so that the Mangler transformation may be employed to transform the variables to an equivalent flat plate. A "compromise" angle which bisects the tip and chord angles of the ogive is assumed. The transformation is illustrated below where the barred quantities denote flat plate variables.

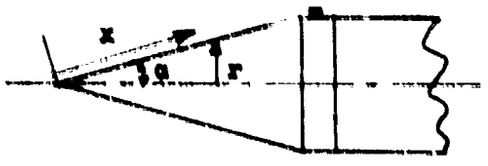

$$r = x\sin\alpha$$

$$\bar{y} = ry$$

$$\bar{x} = 1/3\ x^3 \sin^2\alpha$$

$$\delta = \int_0^{\delta} dy = \int_0^{\bar{\delta}} \frac{1}{r(x)}\, d\bar{y} = \frac{1}{r(x)} \int_0^{\bar{\delta}} d\bar{y} = \bar{\delta}/r(x)$$

The boundary layer thickness for the cone is the flat plate value reduced by $1/r(x)$.

For a flat plate employing the theory of Chapman and Rubesin :

$$\bar{\delta}/2 \sqrt{\frac{U_\infty}{\nu_\infty \bar{x} C}} = 2.5 + .22\ M_\infty^2 + .96\left(\frac{T_w - T_r}{T_\infty}\right)$$

For this analysis an adiabatic wall is assumed with the Chapman constant equal to unity. Thus,

$$\bar{\delta}(\bar{x}) = \frac{(5 + .44\ M_\infty^2)}{\sqrt{u_\infty/\nu_\infty}}\ \sqrt{\bar{x}}$$

and

$$\delta(x) = \frac{\bar{\delta}(\bar{x})}{r(x)} = \frac{(5 + .44\ M_\infty^2)}{\sqrt{u_\infty/\nu_\infty}}\ \frac{\sqrt{\bar{x}}}{x \sin\alpha}$$

Substituting, $\bar{x} = 1/3\ x^3 \sin^2\alpha$ yields :

$$\delta(x) = \left[\frac{(5 + .44\ M_\infty^2)}{\sqrt{u_\infty/\nu_\infty}}\right] \sqrt{x}\ \cdot \sqrt{1/3}$$

This is simply the formula for the flat plate reduced by $1/\sqrt{3}$, <u>except</u>, the conditions on the cone are to be used.

For a free stream Mach number of 5.4, stagnation conditions of 15 kgf/cm^2 and 200°C, and a cone angle of 31° :

M_∞ = 2.5
P_∞ = 0.22 kgf/cm^2
T_∞ = 210°K

The calculated boundary layer thickness at the roughness location (x = 47 mm) becomes :

<u>δ = 0.22 mm</u>.

Upon comparison with schlieren pictures, this value appears conservative.

APPENDIX II

Boundary Layer Calculation for Hollow Cylinder

From theory of Chapman-Rubesin for a flat plate assuming $\gamma = 1.4$:

$$\frac{\delta}{2}\sqrt{\frac{u_\infty}{\nu_\infty x C}} = 2.5 + .22\,M_\infty^2 + .96\left(\frac{T_w - T_r}{T_\infty}\right)$$

where $C = \sqrt{\frac{T_w}{T_\infty}} \times \left(\frac{T_\infty + 102}{T_w + 102}\right)$

For a hollow cylinder whose radius is much greater than the boundary layer thickness the above may be used. The approximate conditions are :

$M_\infty = 5.4$
$T_0 = 200°C$ (nominal value)
$T_w = 100°C$ (assumed)
$T_r = 140°C$ ($r = .848$)
$x = 40$ mm (distance to junction)
$P_0 = 15$ kgf/cm^2

It is interesting to compare the terms on the right hand side (subsonic, compressibility, heating are represented respectively) :

$$\delta/2\sqrt{\frac{u_\infty}{\nu_\infty x C}} = 2.5 + 6.4 - 0.6 = 8.3$$

Finally, $\underline{\delta = 0.75 \text{ mm}}$.

APPENDIX III

An estimation of the boundary layer growth on the flare is presented assuming the Chapman-Rubesin equation :

$$\delta/x \sqrt{\frac{Re_\infty}{C}} = 5 + .44\ M_\infty^2 + 1.92 \left(\frac{T_w - T_r}{T_\infty}\right)$$

The conditions on the flare are approximately :

$M_\infty \sim 3$
$T_\infty \sim 170°K$ (for $T = 200°C$)
$T_r \sim 425°K$

Consider the following ratio for $T_{w_1} = 300°K$ (ambient) and $T_{w_2} = T_r$.

$$\frac{\left(\delta/x \sqrt{\frac{Re_\infty}{C}}\right) t = t_2}{\left(\delta/x \sqrt{\frac{Re_\infty}{C}}\right) t = t_1} = \frac{5 + .44\ M_\infty^2 + 1.92 \left(\frac{T_{w_2} - T_r}{T_\infty}\right)}{5 + .44\ M_\infty^2 + 1.92 \left(\frac{T_{w_1} - T_r}{T_\infty}\right)}$$

or, $\delta_2/\delta_1 = 8.96/7.55 = 1.19$

so the boundary layer growth, $\frac{\delta_2 - \delta_1}{\delta_1}$, is :

$$\frac{\Delta\delta}{\delta} \simeq 20\ \%$$

Note that the boundary layer pitot profiles (fig. 5) indicate a growth of about 30 %.

TEST	MEAN	λ	$\Delta P_p)_{max}$	$\frac{\Delta P_{p\ max}}{P_p}$	STATION	LEADING EDGE	METHOD
F56	-	6.4°-2.1mm	-	-	x_t=30mm	ε=.06mm (new)	sublimation
F110	-	6.7°-2.2	-	-	↓	↓	↓
F225	263mmHg	6.6°-2.2	140mmHg	53 %	↓	↓	pitot survey
F247	524	7.5°-2.5	176	34	↓	ε=.06 (old)	|
F249	425	8.6°-4.6	92	22	x_t=60		|
F260	440	5.7°-1.9	245	56	x_t=30	ε=.02	↓

Leading Edge Condition - Test F260

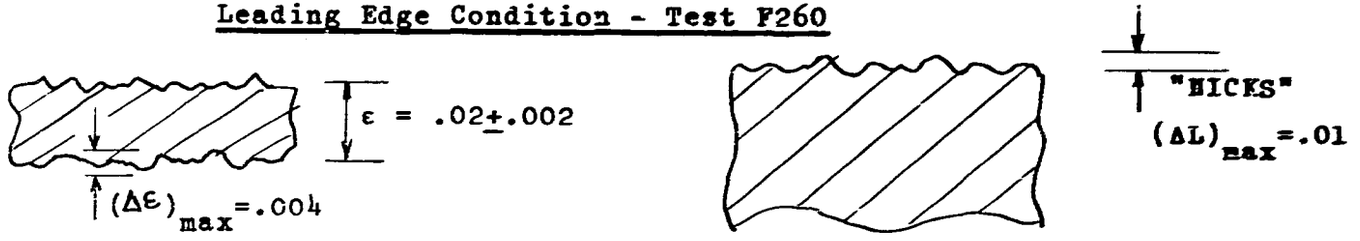

TABLE 1. HOLLOW CYLINDER RESULTS

TEST	RE	MEAN	λ	ΔP_p	$\frac{\Delta P_p}{P_p}$	LOCATION
F234	RE-8	230	10.5°	108	47 %	x_f=30
		190	9.8	95	50	
F235	RE-16	210	9.6	55	26	↓
		189	9.6	42	22	
F236	RE-32	179	10.8	99	55	↓
		174	10.8	101	58	
F237	RE-32	272	11.1	148	54	↓
		269	11.7	145	54	
		261	11.4	138	53	
		237	11.1	101	43	
		230	11.7	105	46	
F238	RE-32	276	11.2	77	28	↓
		272	11.7	100	37	

F239	no roughness	$\frac{255}{210}$	-	4(max)	$\frac{1.6}{1.9}$	x_f=30

F243	RE-32	143	10.5	9	6	before separation
		136	10.6	8	6	y/δ ∿ .75
F245	RE-32	64	11.1	9	14	before
		61	12.3	7	11 $\frac{1}{2}$	separation
		55	11.4	7	13	y/δ ∿ .5

λ

TABLE 2. ROUGHNESS RINGS (RE-8,16,32)

TEST	K	d	MEAN	λ	ΔP_p	$\Delta P_p/P_p$
F251	.164	1.03	157	13.5°	46	29 %
F252	.135	1.04	164	12.6	55	33 ½
	.202	.603	152	11.2	50	33
	.178	.530	133	10.8	49	37 ½
	.164	1.03	172	14.1	66	38 ½
F253	.230	.318	67	9.6	15	21 ½
	.130	.645	64	10.5	18	28
	.178	.530	60	10.8	15	25
F254	.176	.340	185	9.9	11	6
	.230	.318	170	10.2	26	15
	.130	.645	149	9.9	36	24
	.178	.530	127	10.2	24	19
F256	.176	.340	194	9.9	7	4
	.230	.318	181	9.9	24	13
	.130	.645	161	10.2	32	20
	.178	.530	139	10.2	24	17
F258	.164	1.03	185	12.9	56	30
	.210	1.02	206	15.3	77	37 ½
F259	.210	1.02	216	15.3	89	41
	.164	1.03	195	13.2	61	31

TABLE 3. RESULTS FOR ROUGHNESS RING RE-VD8

TEST	d	K	$\frac{\Delta P_p}{P_p}$	$\left(\frac{\Delta P_p}{P_p}\right)_{AVG}$	λ	$(\lambda)_{AVG}$
F259	1.02	.210	41 %	39	15.3°	15.3
F258	↓	↓	$37\frac{1}{2}$		15.3	
F252	1.03	.164	$38\frac{1}{2}$	32	14.1	13.4
F259	|	|	31		13.2	
F258	|	|	30		12.9	
F251	↓	↓	29		13.5	
F252	1.04	.135	$33\frac{1}{2}$	$33\frac{1}{2}$	12.6	12.6

TABLE 4. EFFECT OF ROUGHNESS HEIGHT

K	d	$\Delta P_p/P_p$	$(\Delta P_p/P_p)_{AVG}$	λ	$(\lambda)_{AVG}$
.210	1.02	41	39	15.3	15.3
↓	↓	37 $\frac{1}{2}$		15.3	
.202	.603	33	33	11.2	11.2
.230	.318	21 $\frac{1}{2}$	25	9.6	9.9
↓	↓	15		10.2	
↓	↓	13		9.9	
.164	.103	38 $\frac{1}{2}$	32	14.1	13.4
↓	↓	31		13.2	
↓	↓	30		12.9	
↓	↓	29		13.5	
.178	.503	37	$24\frac{1}{2}$	10.8	10.5
↓	↓	25		10.8	
↓	↓	19		10.2	
↓	↓	17		10.2	
.176	.340	6	5	10.2	10.1
↓	↓	4		9.9	
.135	1.04	33 $\frac{1}{2}$	$33\frac{1}{2}$	12.6	12.6
.130	.645	28	24	10.5	10.2
↓	↓	24		9.9	
↓	↓	20		10.2	

TABLE 5. EFFECT OF ROUGHNESS DIAMETER

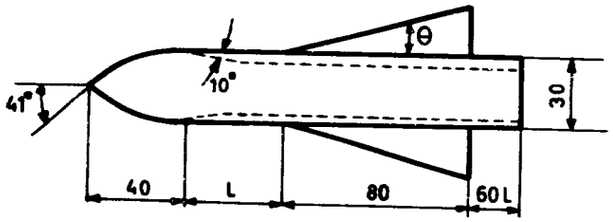

Ogive cylinder (OC I) and hollow cylinder (HC)

Model OC I	Model HC	L mm	θ°
OCI - 1	HC - 1	20	5
- 2	- 2	20	7 1/2
- 3	- 3	20	10
- 4	- 4	40	5
- 5	- 5	40	7 1/2
- 6	- 6	40	10
- 7	- 7	60	5
- 8	- 8	60	7 1/2
- 9	- 9	60	10

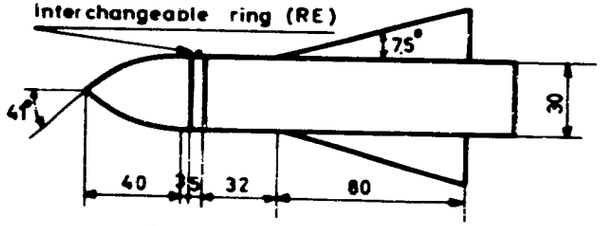

Ogive cylinder (OC II)

Fig. 1 MODELS HC, OCI, OCII

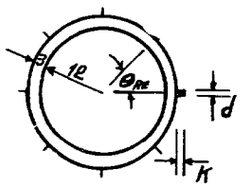

ROUGHNESS RING RE- for OCII, III MODELS

RING	ELEMENT NO. / No. of ELEMENTS	K mm	d mm	θRE °
RE-8	8	.02	.05	45
RE-16	16	↓	↓	22½
RE-32	32	↓	↓	11¼
RE-VDB-	1	.210	1.02	22½
-	2	.164	1.03	↓
-	3	.135	1.04	↓
-	4	.202	.603	↓
-	5	.178	.530	↓
-	6	.130	.645	↓
-	7	.233	.318	↓
-	8	.176	.340	↓

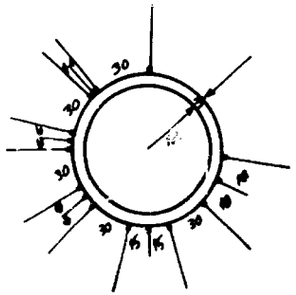

VARIABLE SPACING ROUGHNESS RING RE-VS16- for OCII, III MODELS

{RE Height - K=0.2mm
{RE Diameter - d=0.5mm

FIGURE 2- ROUGHNESS RINGS

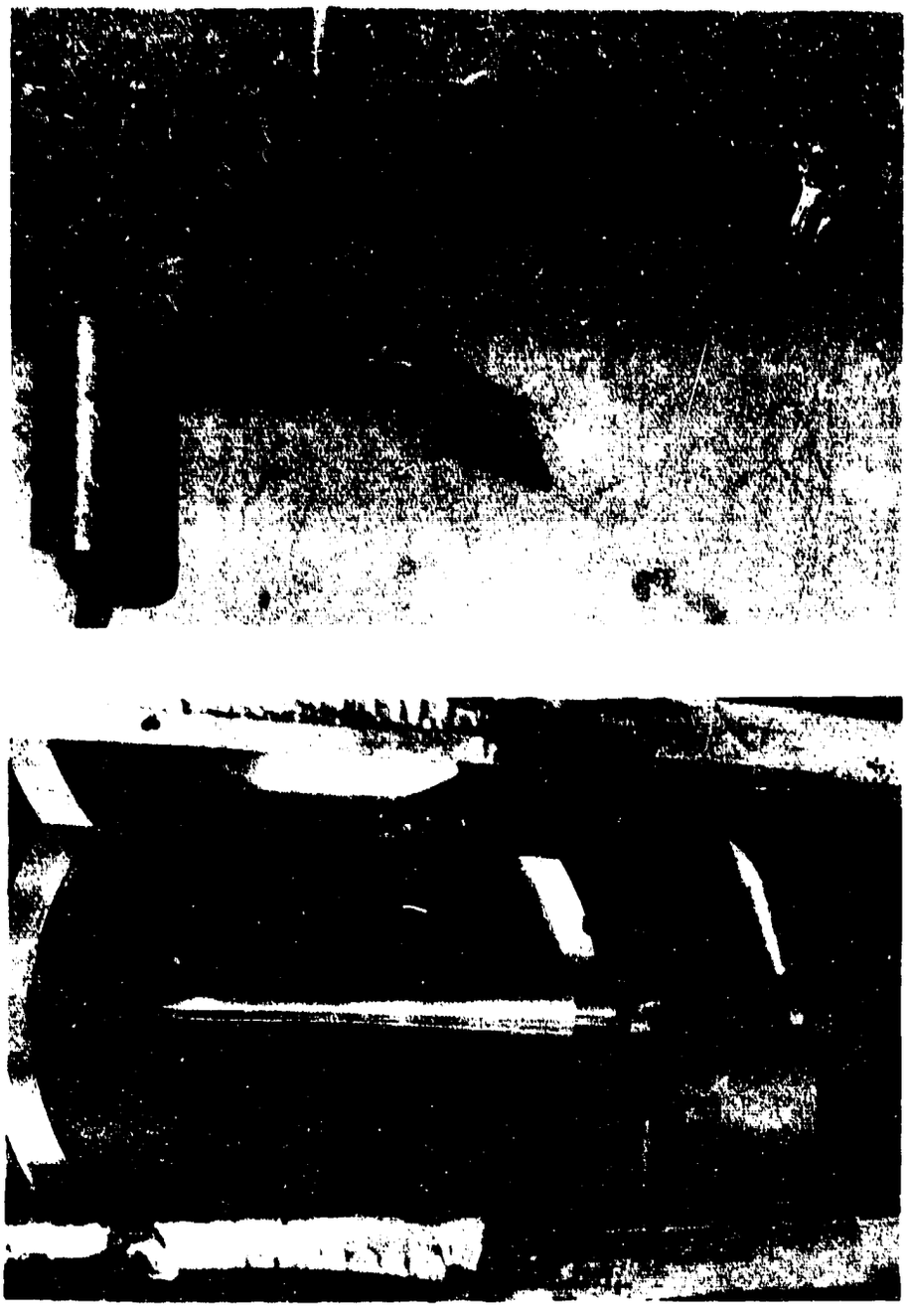

Figure 3- MODEL OCII.

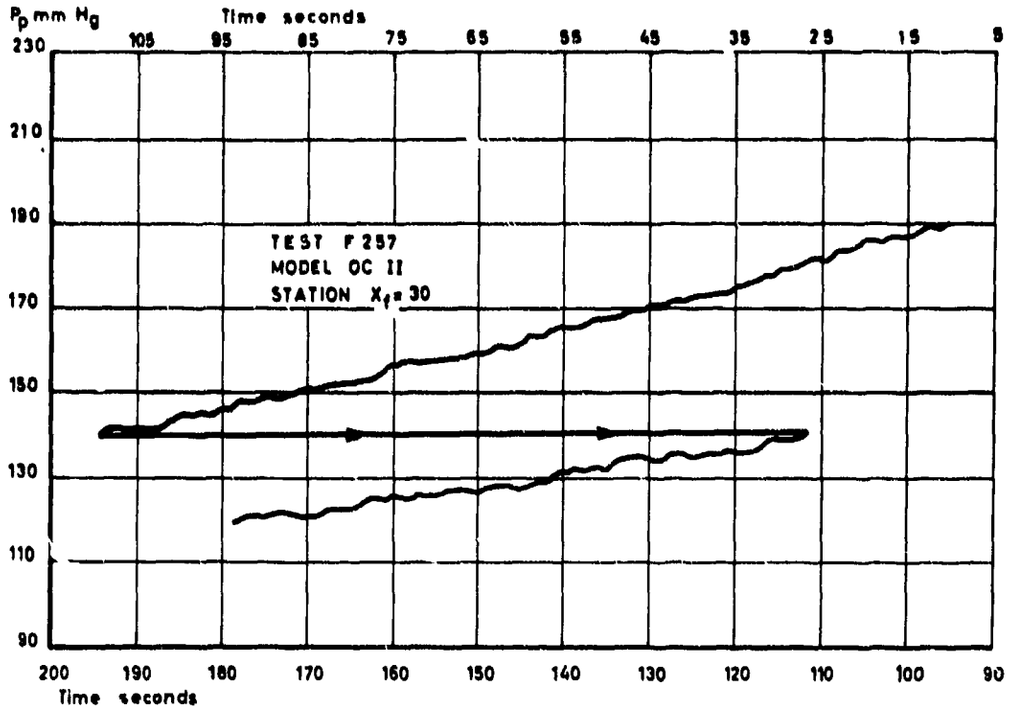

Fig. 4 TEMPERATURE EFFECT ON PRESSURE LEVEL.

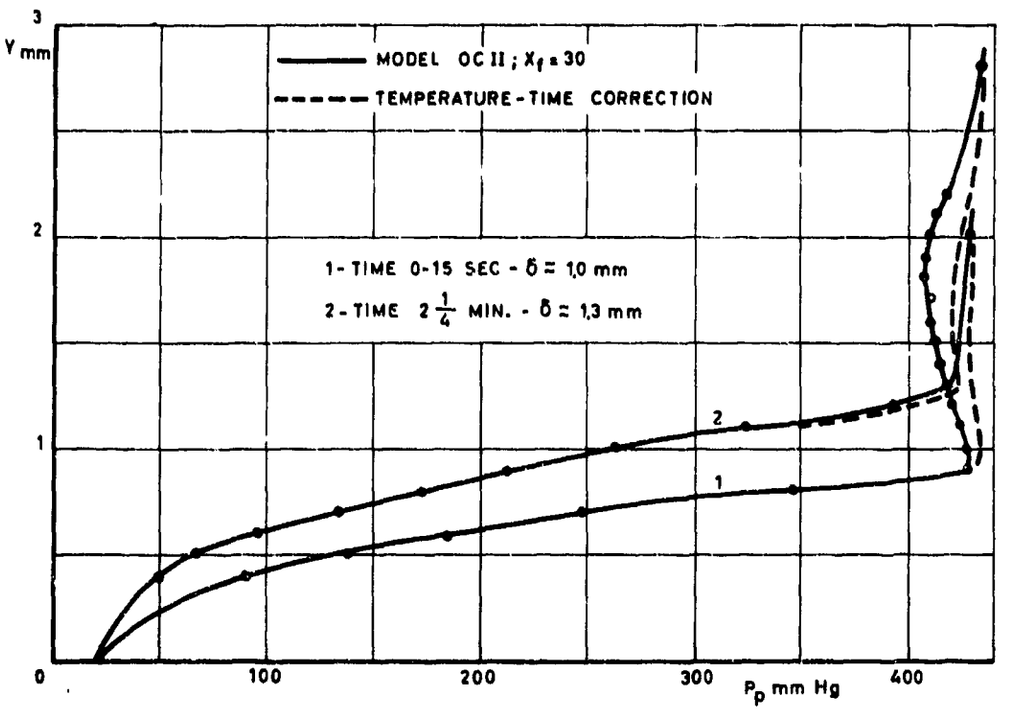

Fig. 5 PITOT PRESSURE PROFILES

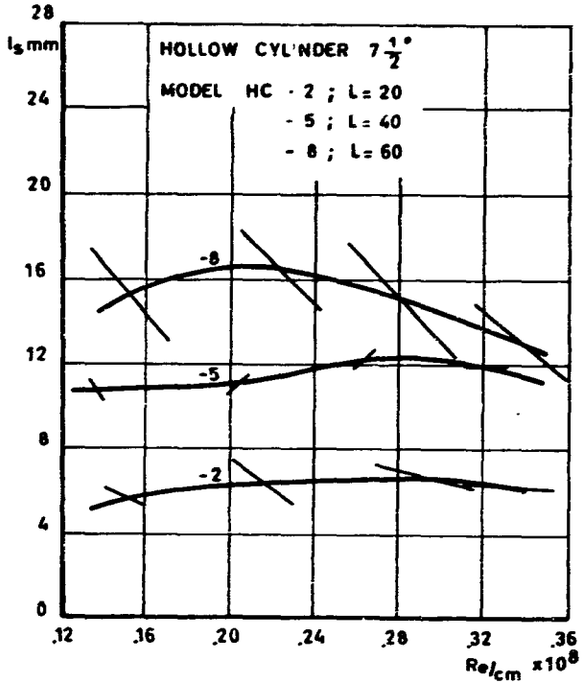

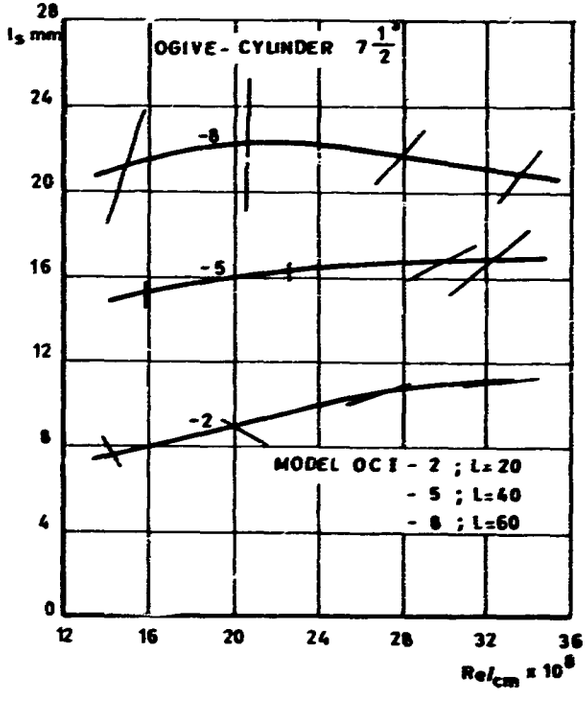

Fig. 6 SEPARATION LENGTH VS REYNOLDS NUMBER

SHADOWGRAPH OF MODEL HC-5.

SCHLIEREN PICTURE OF MODEL HC-5.

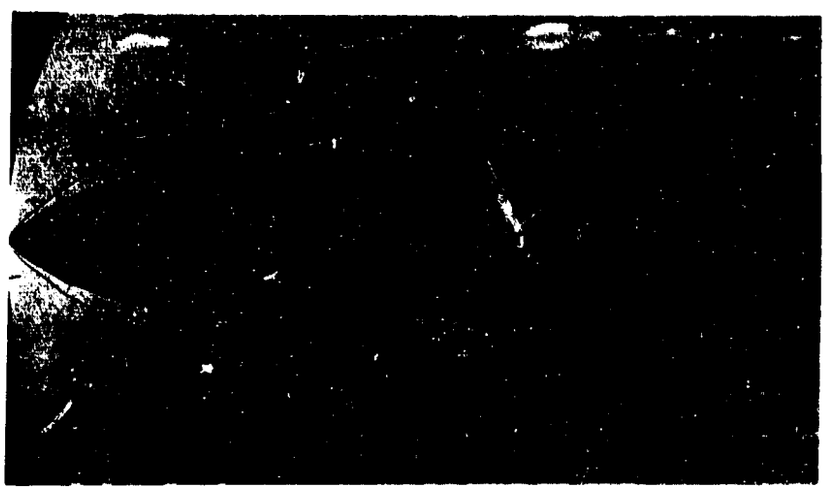

SHADOWGRAPH OF MODEL OC II. Figure 7.

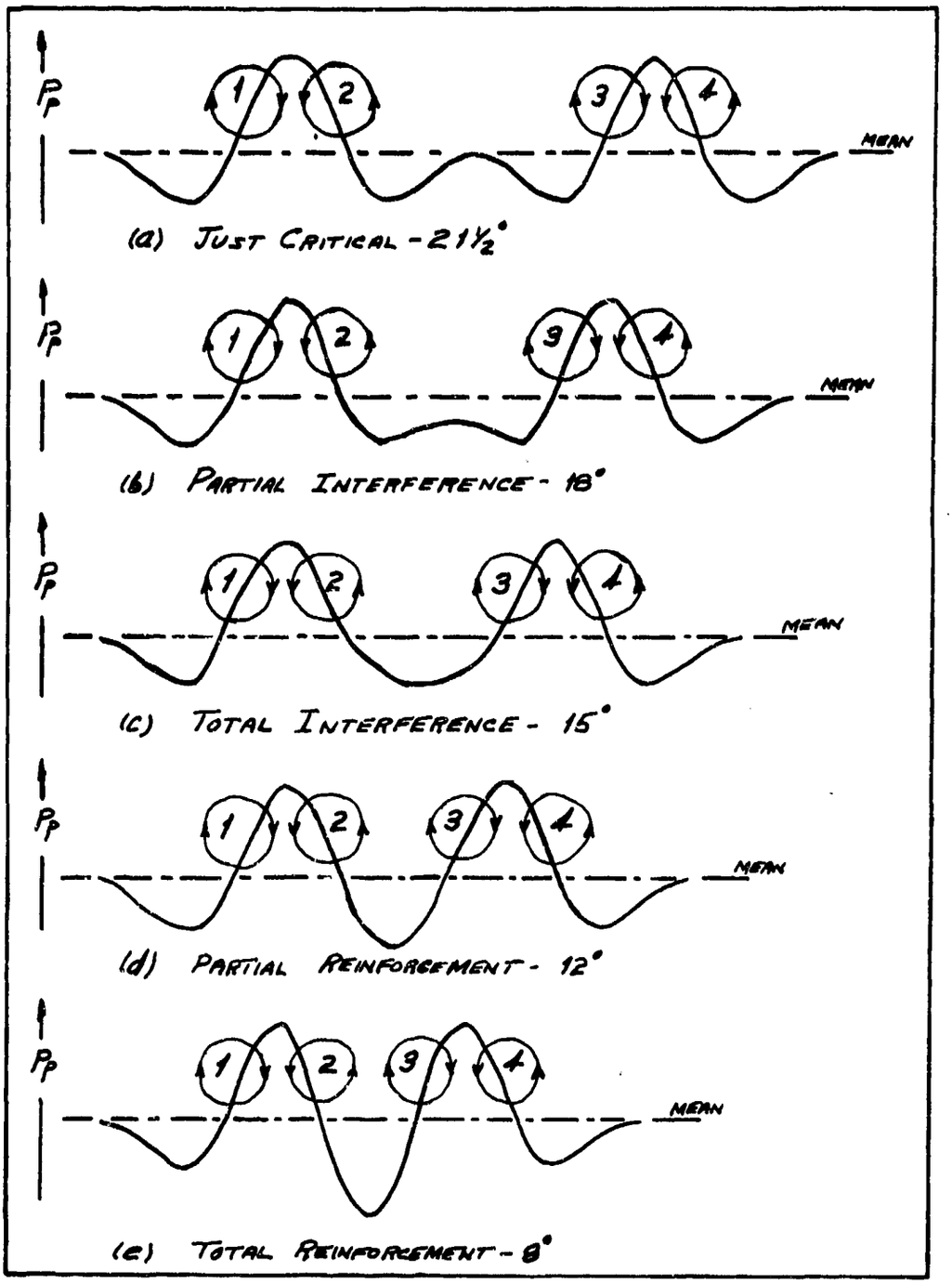

Fig. 8 VORTEX INTERACTION.

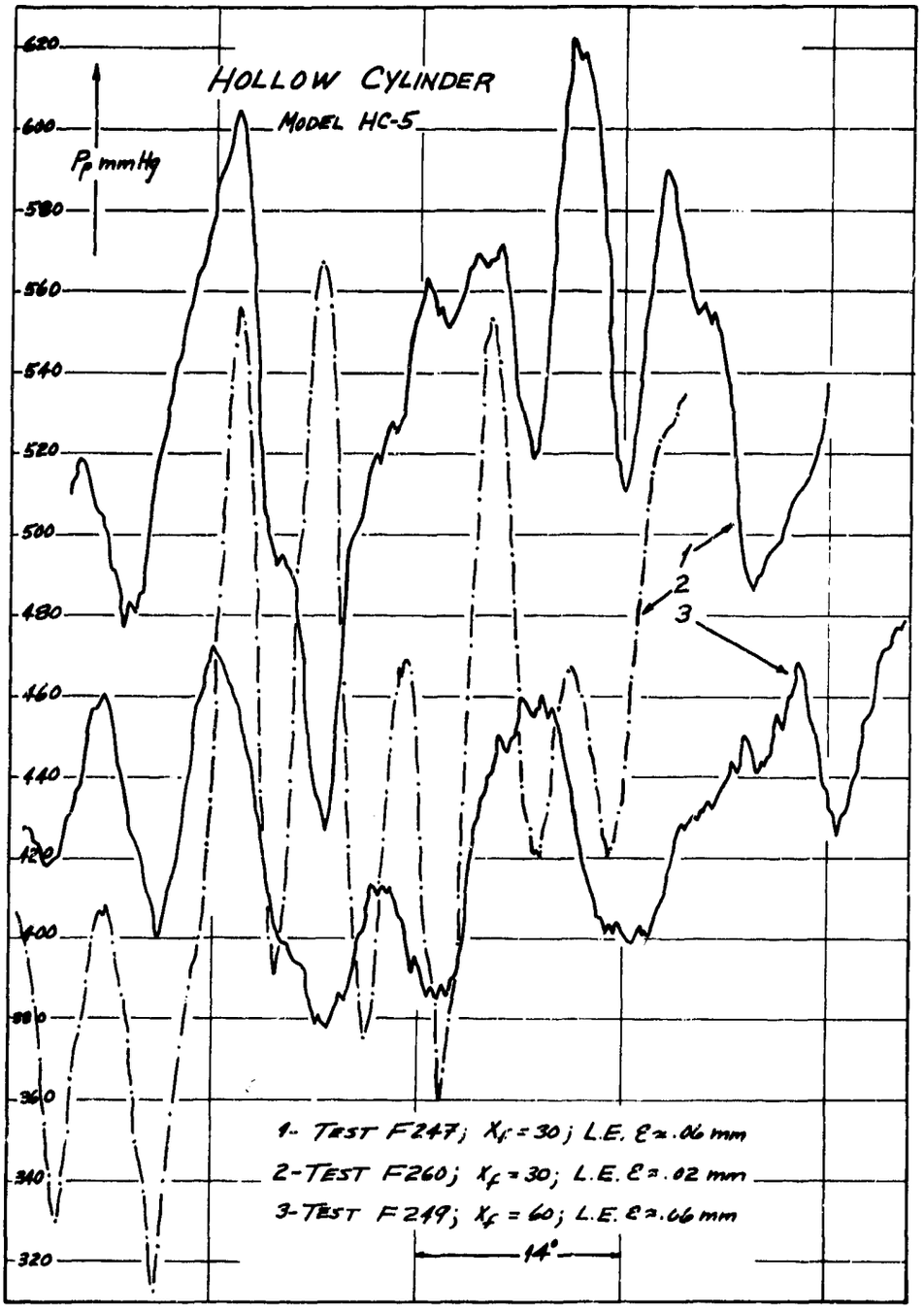

Fig. 9 HOLLOW CYLINDER - PITOT SURVEYS

$P_o = 16.0$ 5° Flare 110 - 90°

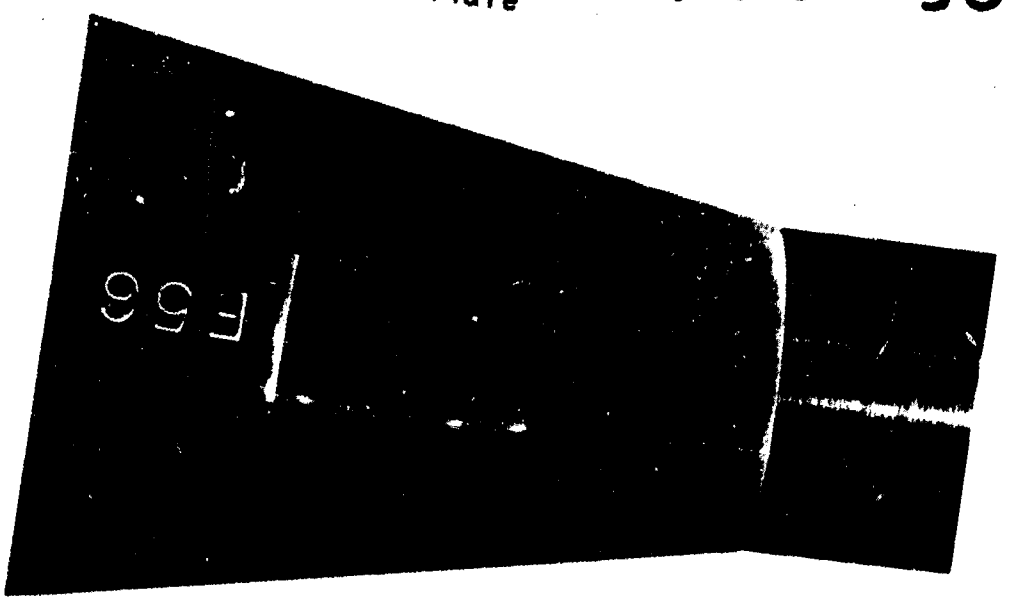

$P_o = 15.6$ 10° Flare

Figure 10 - HOLLOW CYLINDER SUBLIMATION RESULTS.

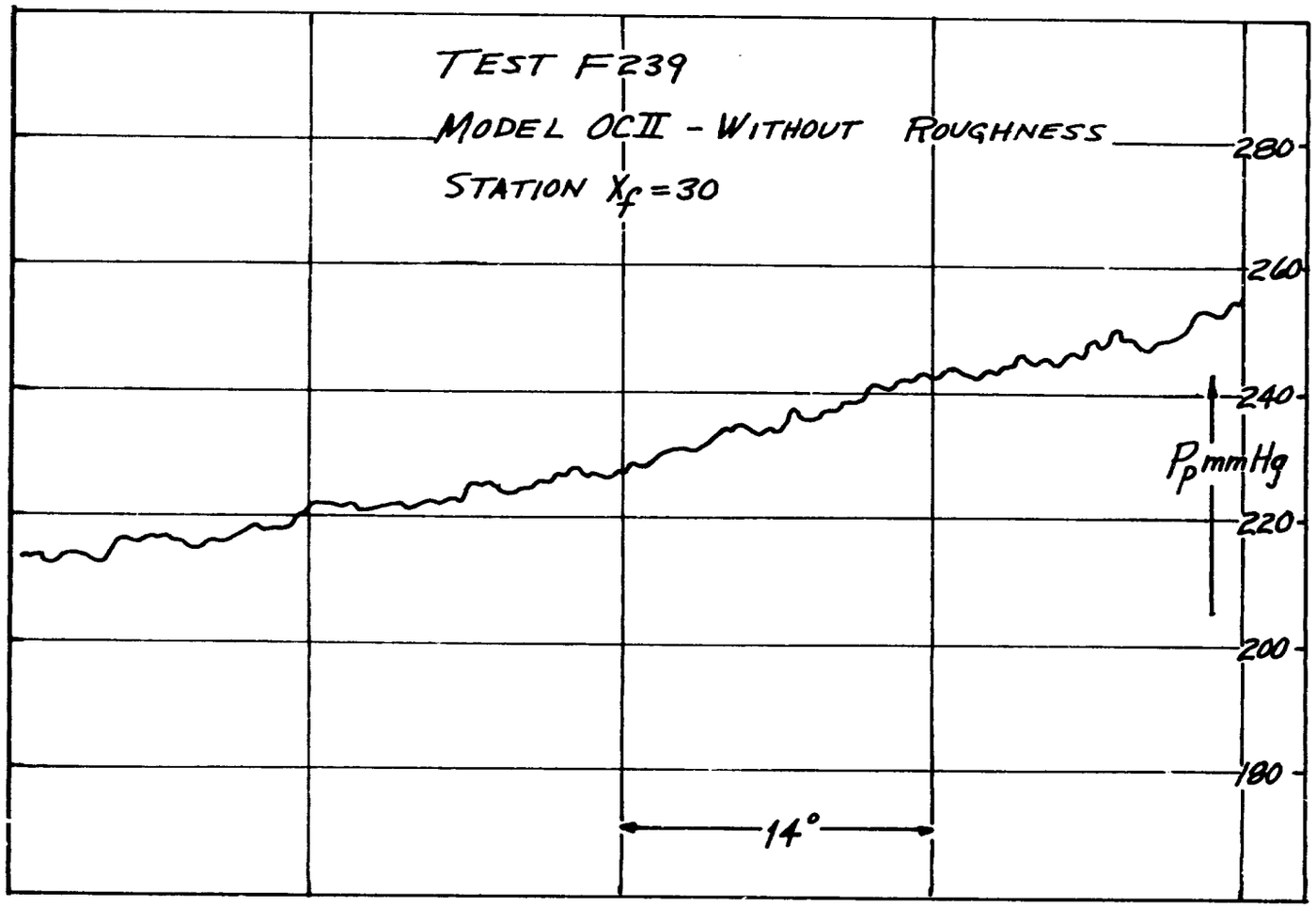

FIGURE 11 - OGIVE CYLINDER - PITOT SURVEY WITHOUT ROUGHNESS

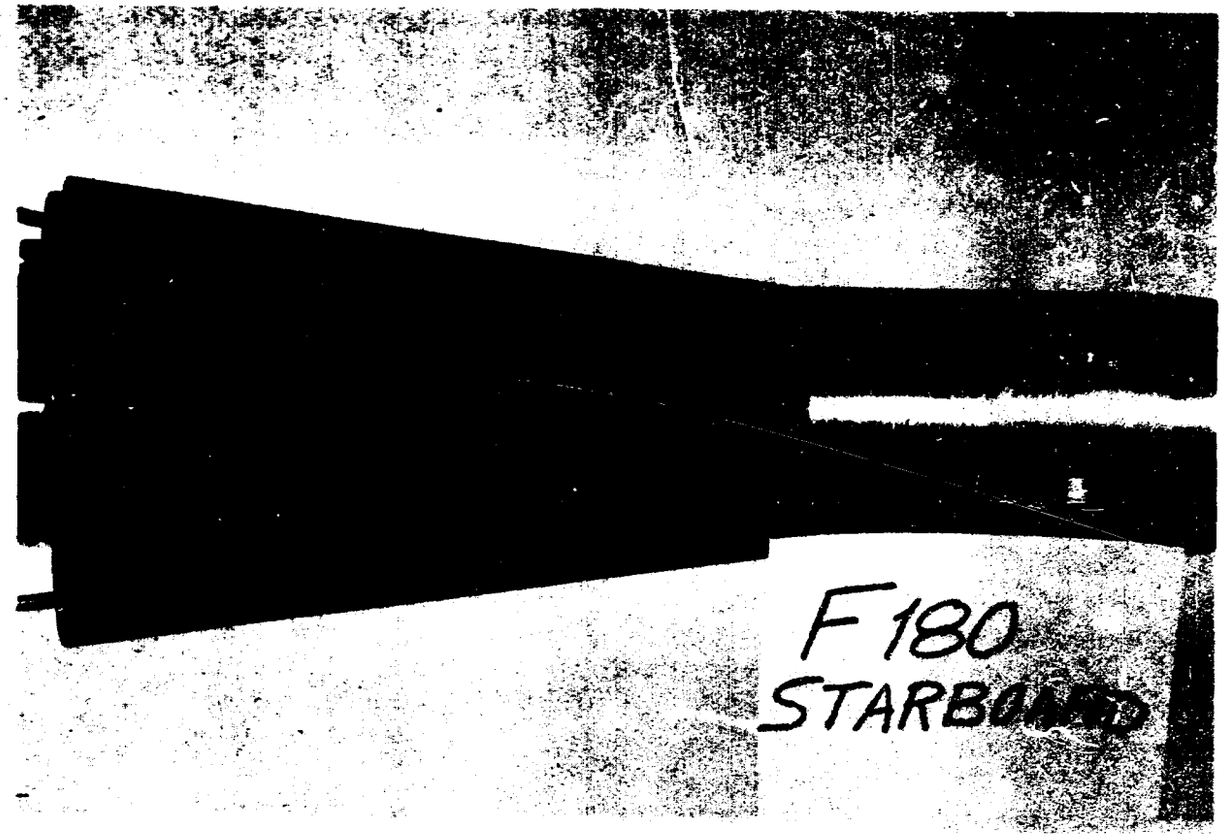

Figure 12 - OGIVE CYLINDER WITHOUT ROUGHNESS.

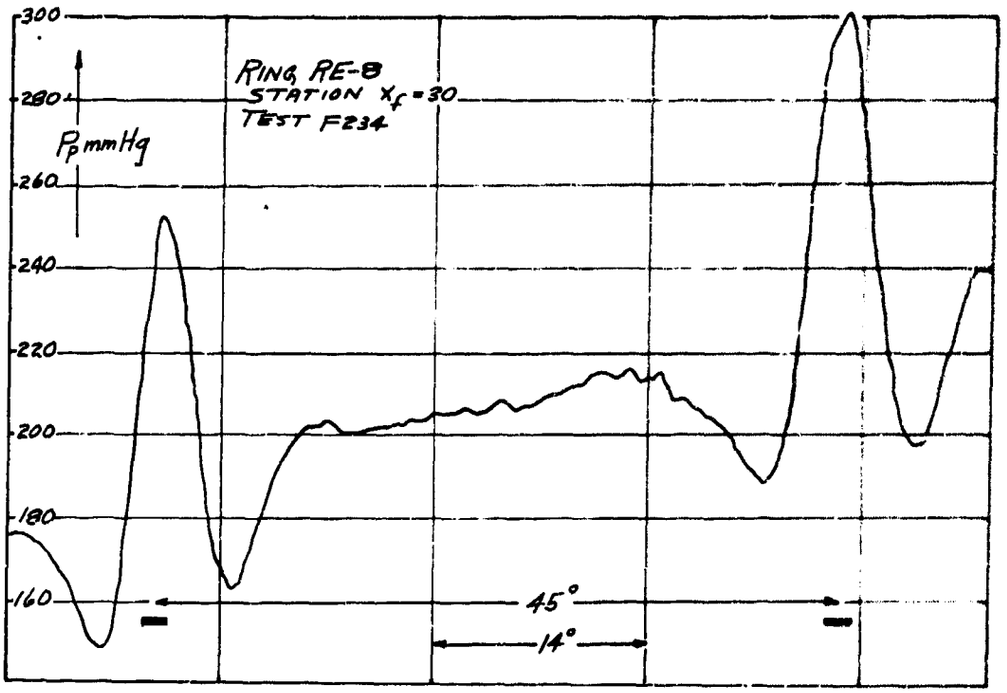

FIGURE 13 - ROUGHNESS RING RE-8 ; PITOT SURVEY

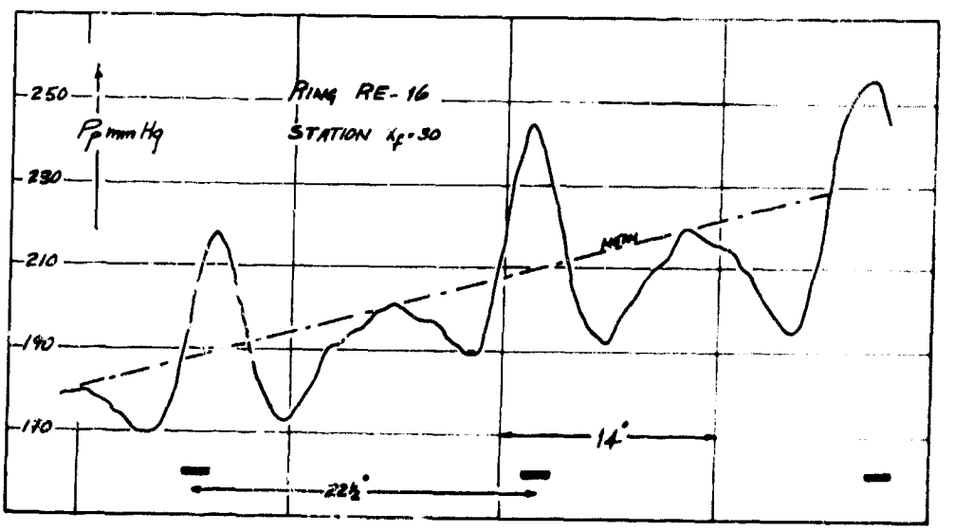

FIGURE 14 - ROUGHNESS RING RE-16 ; PITOT SURVEY

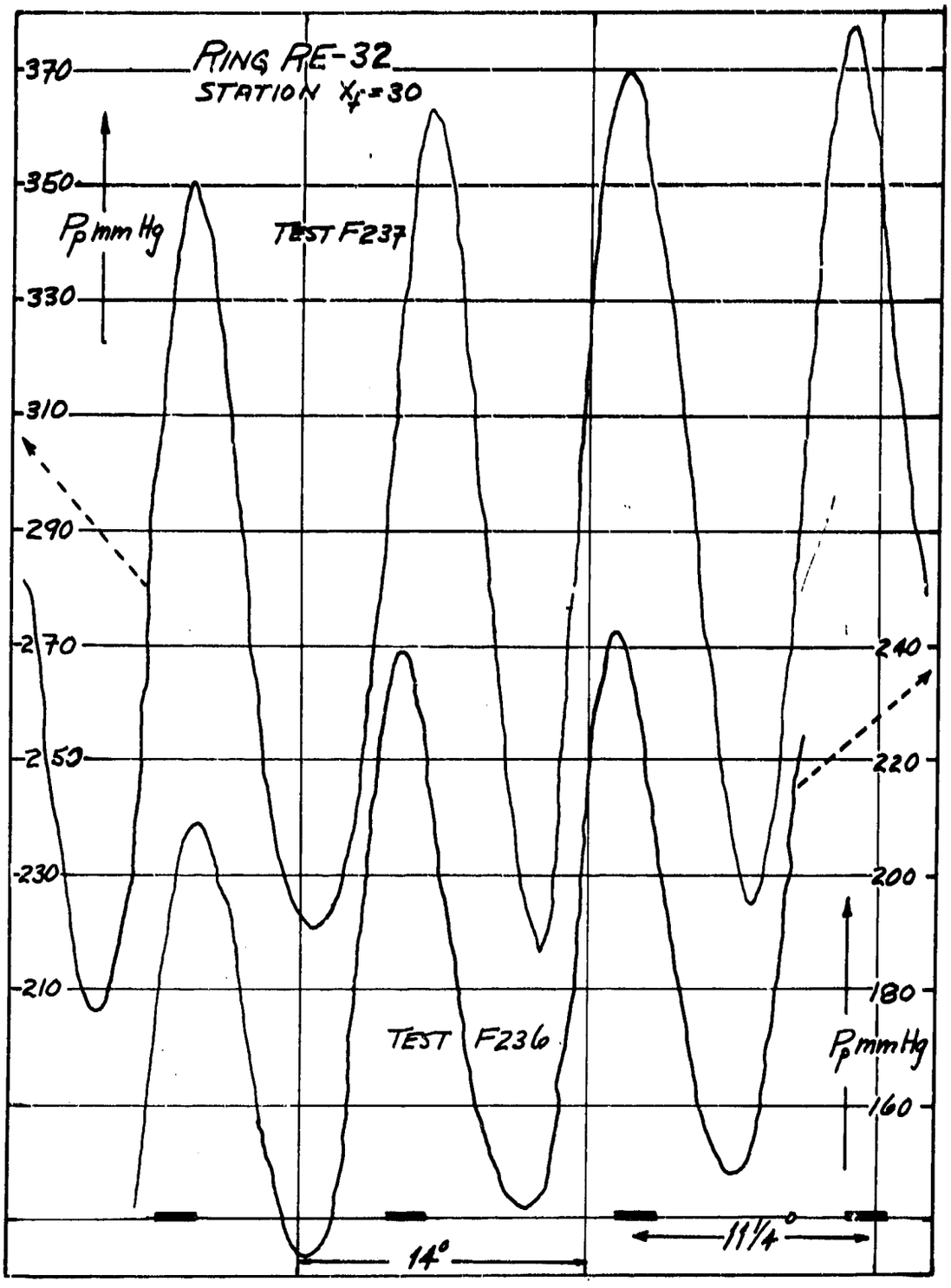

FIGURE 15 - ROUGHNESS RING RE-32 ; PITOT SURVEY

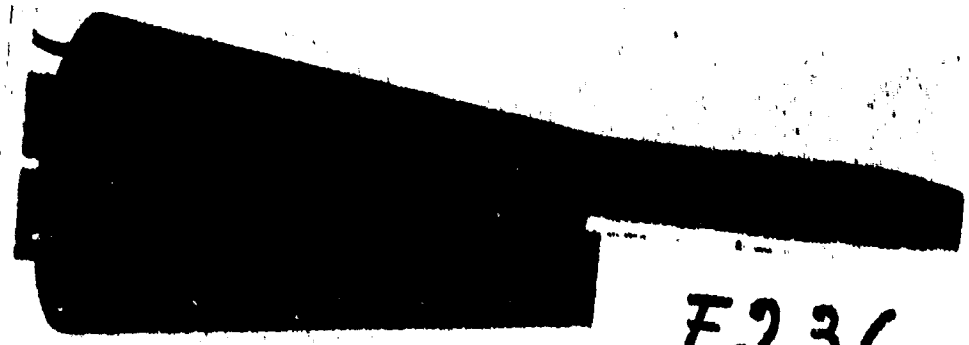

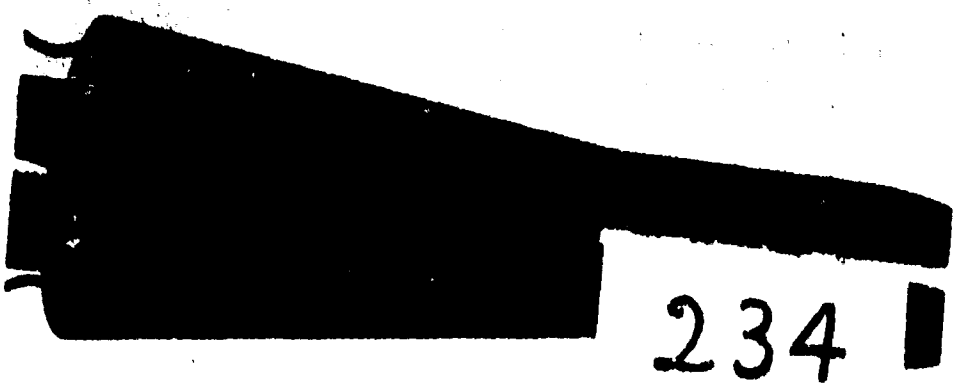

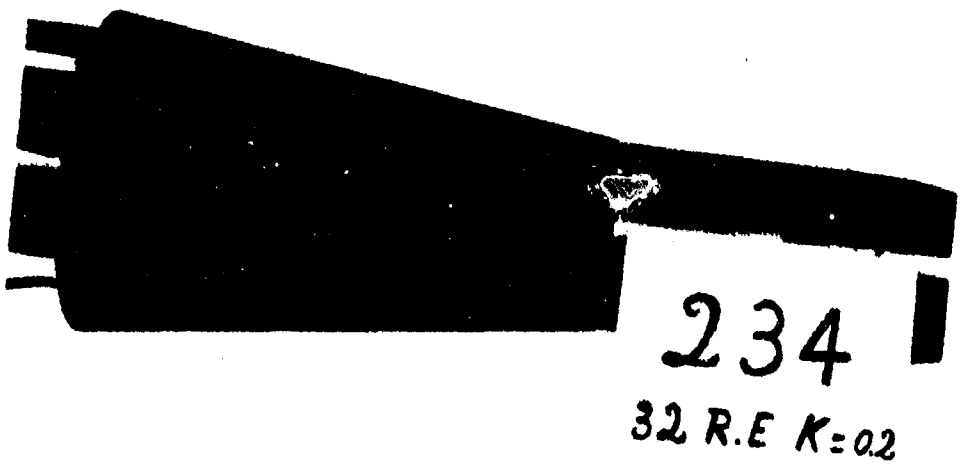

Figure 16.

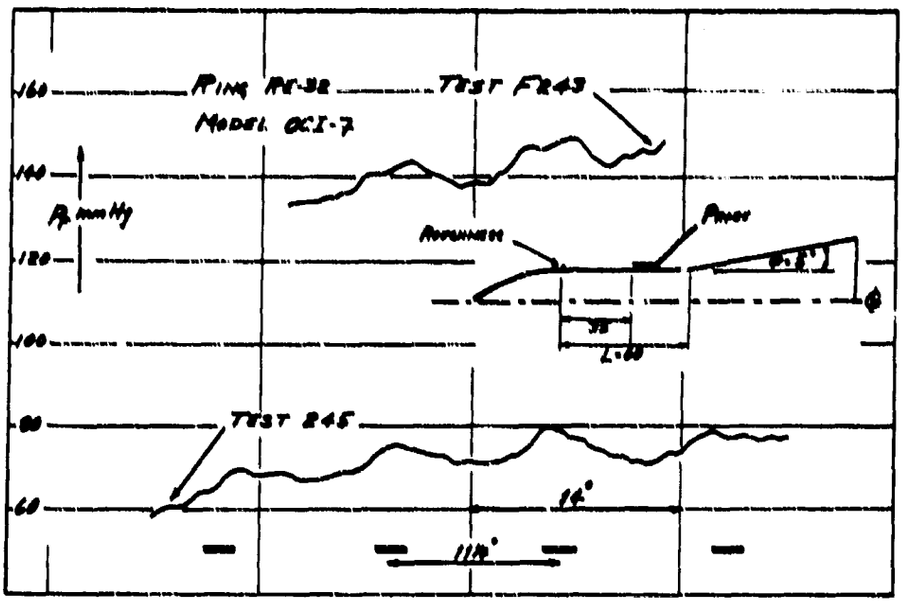

Fig. 17 PITOT SURVEY UPSTREAM OF SEPARATION

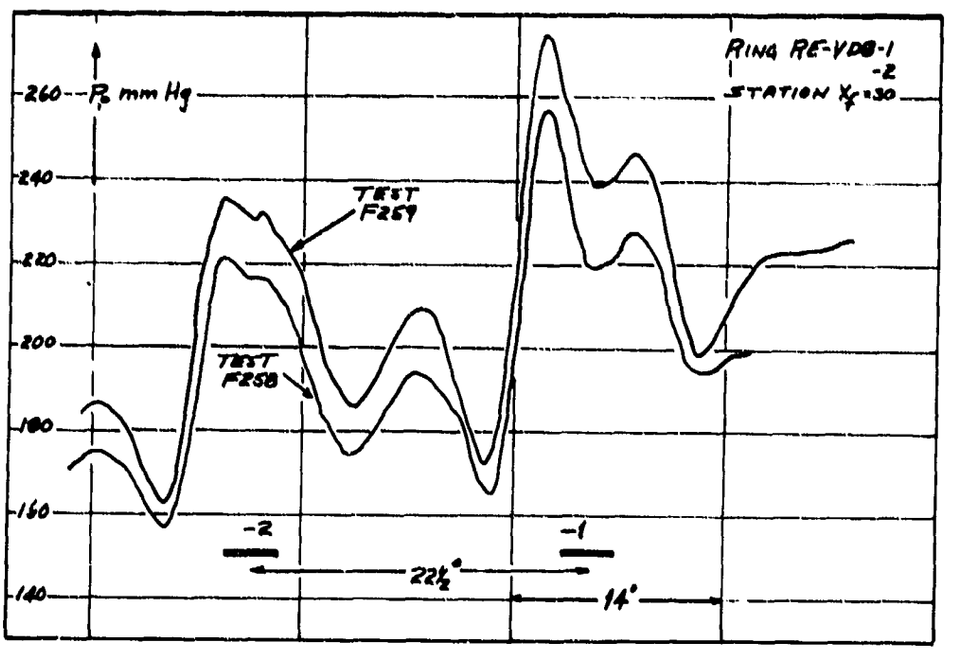

FIGURE 18 - ROUGHNESS RING RE-VDB-42 ; PITOT SURVEY

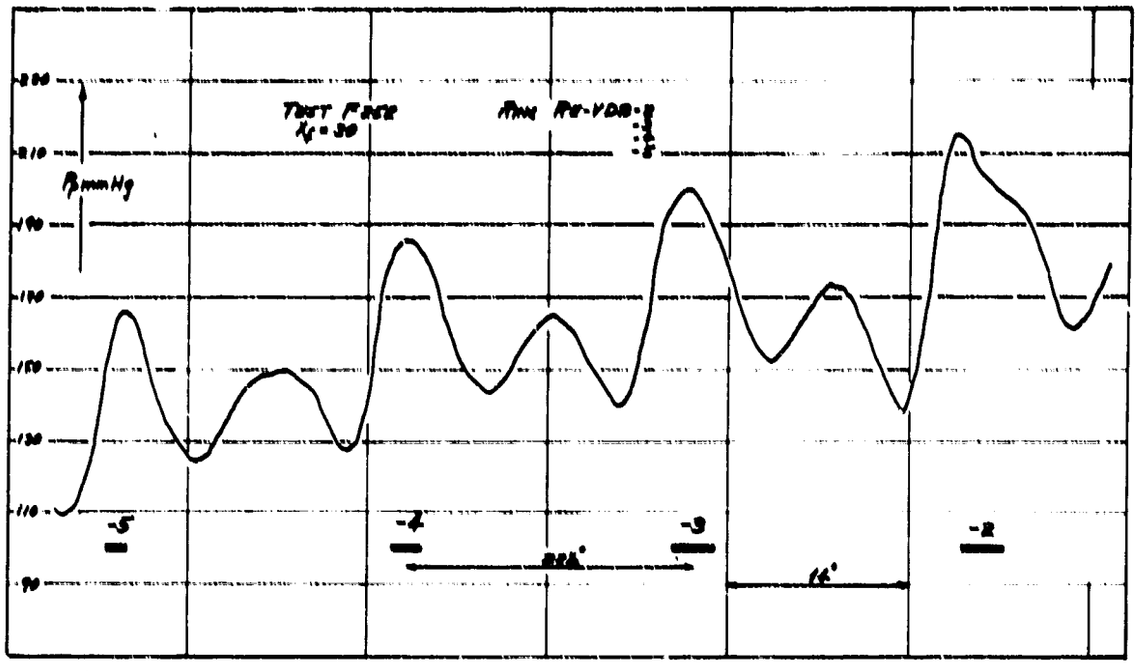

FIGURE 19 - ROUGHNESS RING RE-VDB-2,3,4,5 - PITOT SURVEY

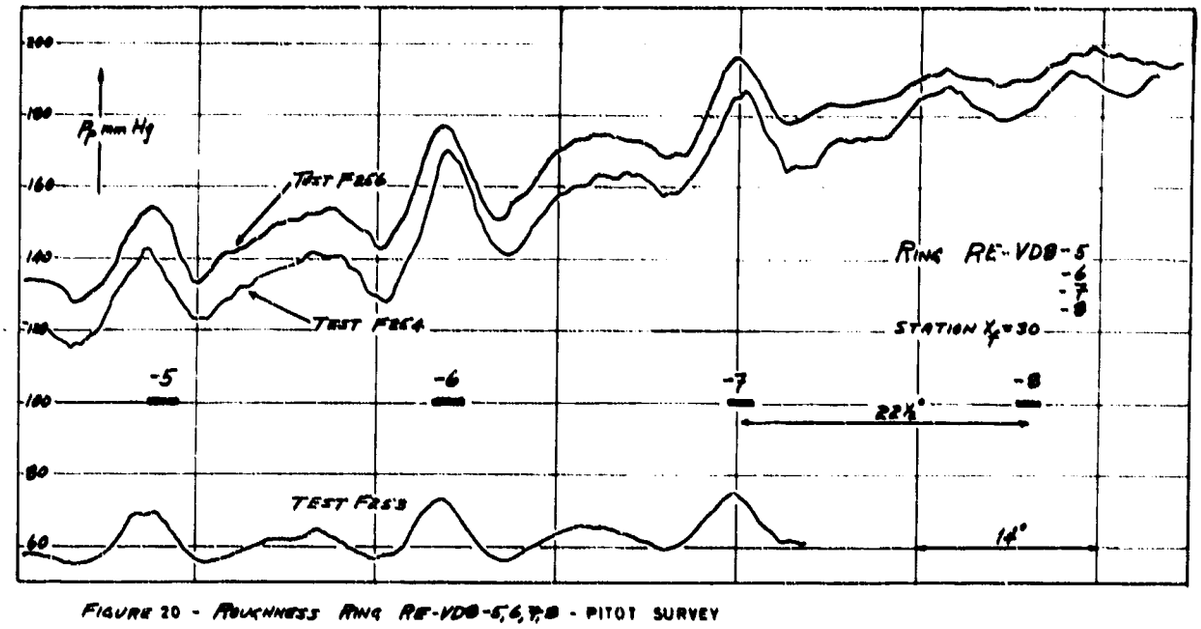

FIGURE 20 - ROUGHNESS RING RE-VDB-5,6,7,8 - PITOT SURVEY

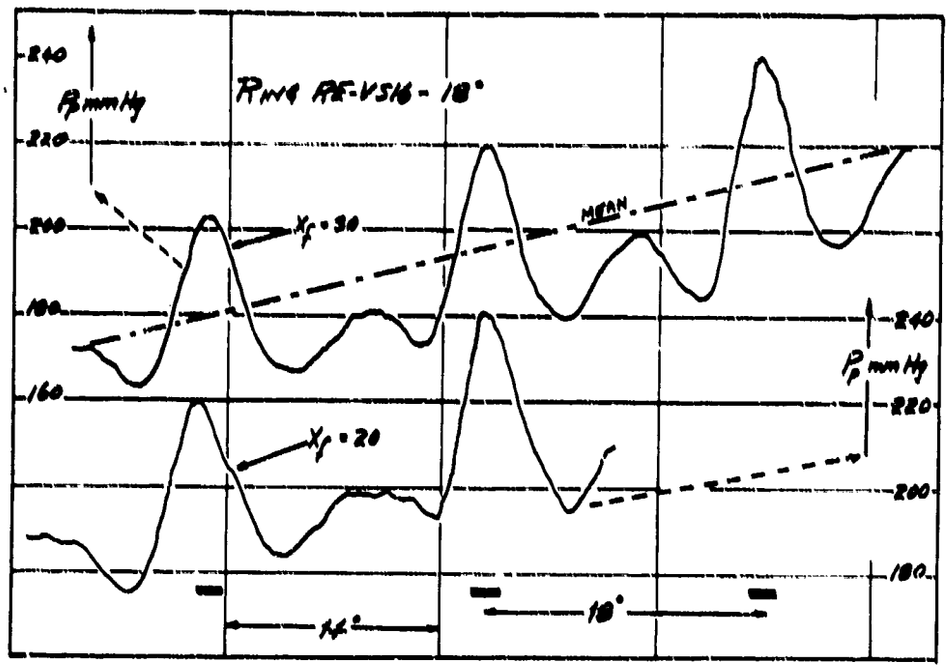

FIGURE 21 - ROUGHNESS RING RE-VS 16-18°; PITOT SURVEY

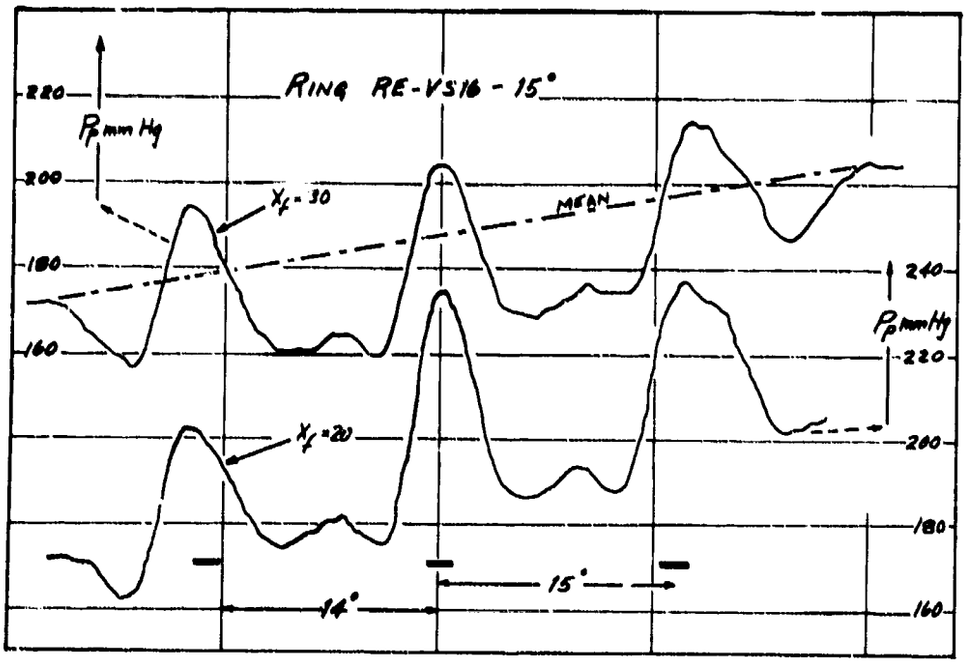

FIGURE 22 - ROUGHNESS RING RE-VS16-15°; PITOT SURVEY

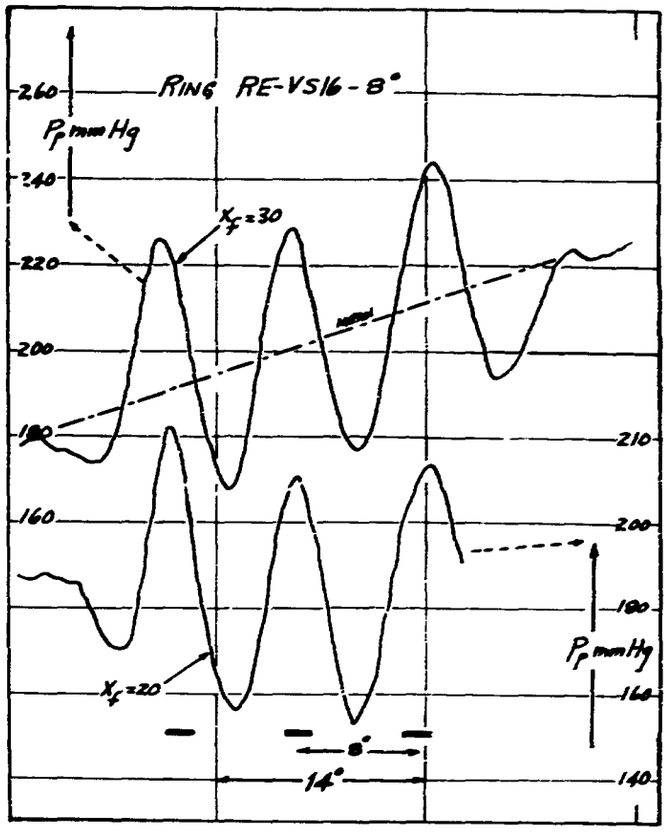

FIGURE 23 - ROUGHNESS RING RE-VS16-8°
-PITOT SURVEY

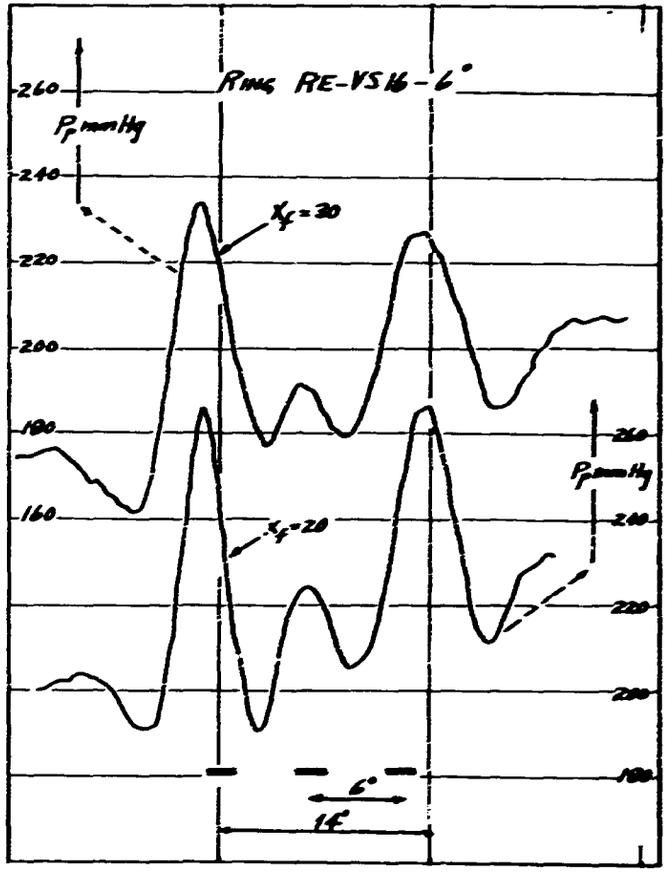

FIGURE 24 - ROUGHNESS RING RE-VS16-6°
-PITOT SURVEY

AD 674 003

von Karman Institute for Fluid Dynamics

ERRATA

Technical Note 41

page ii 3rd line: M = 5.3 should read M = 5.4

vi 12th line: corss section should read cross-section

vii 2nd line: page 24 should read page 25

12 14th line: appendix IV should read appendix III

13 14th line: (for the most common size (K = .2, d = .5)
should read: (for the most common size; K = .2 ..

21 top sketch u_1 and u_2 should read $\vec{u}_1$ and $\vec{u}_2$

22 bottom sketch: $\frac{\partial u}{\partial y}_A < \frac{\partial u}{\partial y}_B$ is true for small y or as y→0

29 last line: a light-dark-light contract should read
a light-dark-light contrast

34 last line: figure 8c should read figure 8d

35 28th line: a respectable should read a repeatable

Table 5: 2nd column, 8th row: .103 should read 1.03

Figure 16: 2nd photograph: 234 should read 235

ARIN-GHOUSE
Scientific & Technical